PERGAMON

Deep-Sea Research II 50 (2003) 769–798

DEEP-SEA RESEARCH
PART II

www.elsevier.com/locate/dsr2

Modeling controls of phytoplankton production in the southwest Pacific sector of the Southern Ocean

Katja Fennel*, Mark R. Abbott, Yvette H. Spitz, James G. Richman, David M. Nelson

College of Oceanic and Atmospheric Sciences, Oregon State University, Corvallis, OR 97331, USA

Accepted 10 March 2002

Abstract

The Southern Ocean is the largest high-nutrient, low-chlorophyll region in the world's ocean and a potentially important site for the sequestration of carbon. We present a one-dimensional physical/biogeochemical model that integrates biogeochemical measurements obtained during the AESOPS (U.S. JGOFS) study in the southwest Pacific sector to elucidate the controls of primary productivity and export. The model is applied to a series of four stations along 170°W spanning the different biogeochemical subsystems in the Polar Frontal Zone, the Polar Front, and the Seasonal Ice Zone south of the Polar Front. Since horizontal fluxes of heat, freshwater and nutrients are found to be important but cannot be resolved explicitly in a one-dimensional model, we employ a restoration of temperature, salinity and nutrients. The surface fluxes of light and momentum are modified during ice-covered periods to account for the effects of sea ice. The biological model component includes the elemental cycles of nitrogen and silica. Diatoms are represented as a separate phytoplankton group, and small phytoplankton and zooplankton are tightly coupled. The effect of the low iron availability in the region is implicitly taken into account by using typical phytoplankton growth rates and a typical, high Si:N stoichiometry of 4 for the diatoms. The model captures the essential features of the distinct subsystems including the low-chlorophyll condition north of the Polar Front, the diatom blooms in the vicinity of the Polar Front and to its south, the differential drawdown of nitrate and silicic acid, and the seasonal patterns of biogenic silica, primary production and vertical particle flux. "Top-down" control of the small phytoplankton by efficient microzooplankton grazing and "bottom-up" control of diatoms by light and silicic acid are the main factors for the simulated behavior. A sensitivity analysis of the biological model component shows that the growth parameters for the two phytoplankton groups are most important in constraining primary productivity and overall model behavior. This implies that changes in growth rates induced by variations in iron supply as assumed over glacial–interglacial transitions can affect primary and export production substantially.

1. Introduction

The Southern Ocean, located between the Subtropical Front (STF) at approximately 45°S and Antarctica, is considered the largest high-nutrient, low-chlorophyll (HNLC) region in the

*Corresponding author. Current address: IMCS, Rutgers University, New Brunswick, NJ 08901, USA. Tel.: +1-732-932-6555; fax: +1-732-932-8578.

E-mail address: kfennel@imcs.rutgers.edu (K. Fennel).

0967-0645/02/$ - see front matter
PII: S0967-0645(02)00594-5

world's ocean and is an important site for the biogeochemical cycles of carbon and silica. Because of the large reservoir of unused macronutrients in the surface waters of the Southern Ocean, it is potentially important for the sequestration of carbon and probably of disproportionate influence on carbon cycling in the changing global ocean. Several factors, including light, grazing and iron, are thought to be important in regulating primary and export production in the Southern Ocean, but the degree to which each factor contributes to the high-nutrient, low-chlorophyll regime is not fully resolved yet.

The size and remoteness of the Southern Ocean make it one of the most poorly sampled oceanic regions. Important characteristics of the biogeochemical system such as the limitation of productivity, the coupling between primary producers and grazers, and the magnitude of export production are still poorly constrained. Most discussions about the HNLC phenomenon and the potential role of the region in carbon cycling involve the iron hypothesis. As formulated by Martin and Fitzwater (1988) the iron hypothesis suggests that phytoplankton growth is currently limited by iron deficiency and that the level of primary and export production has been much higher during periods with higher airborne iron deposition, e.g., during glacial periods. Competing hypotheses emphasize the role of light and grazing in constraining production (Mitchell et al., 1991; Frost, 1991; Cullen, 1991), and it is now generally understood that an interplay of factors controls primary productivity in the Southern Ocean. Iron exerts selective pressure on larger size classes, namely diatoms, but light, silicic acid concentrations, and grazing play key roles as well (de Baar and Boyd, 2000; Cullen, 1995). It remains to be seen to what degree iron controls primary and export production.

The Antarctic Environment Southern Ocean Process Study (AESOPS) was initiated as part of the U.S. JGOFS program with the ultimate goal to better constrain the fluxes of carbon in the Southern Ocean and to gain sufficient understanding to predict its response to future global changes. AESOPS focused on the southwestern Pacific sector to identify the factors and processes that regulate the magnitude and variability of primary productivity and the fate of biogenic material in this region. A series of four cruises, spanning the Antarctic Circumpolar Current (ACC) at $\sim 170^{\circ}$W, was conducted between October 1997 and February 1998, providing a valuable data set of seasonal and spatial patterns of the chemical and biological properties. Several recent findings partly obtained within AESOPS challenge the common notion of the Southern Ocean as a HNLC region. North of the Polar Front silicic acid concentrations reach limiting levels in summer, leading to a more accurate characterization of that area as a low-silica, high-nitrate region (Dugdale et al., 1995). In the vicinity of the Polar Front phytoplankton blooms and chlorophyll levels of ~ 2 mg m^{-3} have been observed in association with physical features like meandering fronts (Barth et al., 2001; Abbott et al., 2000; Moore et al., 1999b). South of the Polar Front an intense seasonal diatom bloom and high silica production rates have been reported, and the corresponding depletion of silicic acid concentrations in the euphotic zone is 30 to $>$ 40 mmol Si m^{-3} (Brzezinski et al., 2001). Furthermore, substantial export of biogenic material is observed. Relatively high and uniform fluxes of organic carbon, twice as high as the estimated ocean-wide average, occur in the Polar Frontal Zone and the Antarctic zone (Honjo et al., 2000).

The emerging picture of the Southern Ocean as a physically and biogeochemically dynamic region with a mosaic of regulating factors implies that simple estimates and extrapolations of its biogeochemical impact cannot be made. Attempts to model the system and to predict future changes need to consider the potentially important factors and mechanisms and should be able to capture shifts and feedbacks in biogeochemical cycling. Ecological models have been developed for different section of the Southern Ocean by Pondaven et al. (2000, 1998), Hense et al. (2000), and Lancelot et al. (2000). The models differ in ecological complexity and vertical resolution. Hense et al. (2000) and Lancelot et al. (2000) have run zero-dimensional models and focus on the Polar Front regime in the Atlantic sector of the Southern Ocean. The one-dimensional model of

Pondaven et al. (2000, 1998) was run at the KERFIX station in the permanently ice-free zone south of the Polar Front in the Indian sector. A common feature of all these models is the inclusion of the nitrogen and silica cycles. In terms of model complexity the models of Hense et al. (2000) and Pondaven et al. (2000, 1998) are kept relatively simple, containing 7–11 state variables, while the model of Lancelot et al. (2000) is rather complex, with about 30 state variables including phosphorus and iron as additional nutrients. We present a model that is focused on a latitudinal transect in the southwest Pacific sector of the Southern Ocean spanning the Polar Frontal Zone, the Polar Front, and the Seasonal Ice Zone. The model is deliberately designed to be simple but includes the cycling of nitrogen and silica. It is intended to be general and flexible to capture the essential features of the different subsystems by resolving the underlying environmental controls. Our objective in this modeling study is an integration of the biogeochemical measurements from the AESOPS field study to elucidate the controls of primary productivity in the study area.

2. Physical and biochemical features of the southwestern Pacific sector

The prominent circulation feature of the Southern Ocean is the Antarctic Circumpolar Current (ACC), which flows eastward around Antarctica, connecting all major oceans. The ACC transports roughly 100×10^6 m^3 s^{-1} (Orsi et al., 1995). The flow is concentrated in narrow jets, coinciding with the principal fronts, which are characterized by strong mesoscale variability (Barth et al., 2001) and interspersed with broader bands of reduced or even reversed flow (Daly et al., 2001). The three major fronts of the ACC from north to south are the Subantarctic Front, the Polar Front (PF) and the Southern ACC Front (Orsi et al., 1995). The water masses separated by these zonally oriented fronts extend around the whole circumpolar path, forming a relatively homogeneous environment in the zonal direction. The PF represents a hydrographical boundary that separates distinct biogeochemical subsystems—the Polar Frontal Zone (PFZ) north of the PF and south of the Subantarctic Front (SAF; Orsi et al., 1995) and the Seasonal Ice Zone (SIZ) south of the PF (Trèguer and Jacques, 1992). The seasonal ice cover in the SIZ strongly affects the light conditions by increased albedo and light attenuation within the ice. Freshwater input during ice melt enhances stratification in spring. The SIZ is rich in macronutrients due to the upwelling of Circumpolar Deep Water. Winter concentrations of surface nitrate and silicic acid are $\sim$30 mmol N m^{-3} and $\sim$60 mmol Si m^{-3}, respectively. In spring after stratification, an intense diatom bloom follows the quickly retreating ice edge (Brzezinski et al., 2001). Franck et al. (2000) report a switch in the relative importance of regulating nutrients in this area from iron before and during the diatom bloom to silicic acid after the bloom.

North of the PF, the mixed-layer depths are generally deeper and stratification is less pronounced. Nitrate levels are high with winter surface concentrations between 20 and 25 mmol N m^{-3}, but surface concentrations of silicic acid are significantly lower than south of the PF, with concentrations between 10 and 15 mmol Si m^{-3}. Chlorophyll levels are low and stable throughout the year and no intense blooms are observed (Banse, 1996). Macronutrients are drawn down to some extent during summer, in particular silicic acid, which reaches concentrations low enough to limit diatom production (Daly et al., 2001). The phytoplankton community is dominated by pico- and nanoplankton.

The PF separates the subsystems but also has its own distinctive features. The high mesoscale variability associated with the ACC jets and fronts induces localized upwelling of nutrients and patches of increased stratification. Both contribute to favorable growth conditions for phytoplankton and lead to a short-lived seasonal high production signal (Abbott et al., 2000) creating localized patches of high chlorophyll (Barth et al., 2001). On satellite images the PF appears as a band of high chlorophyll (Moore et al., 1999a). Observations of bio-optical characteristics show that phytoplankton are initially limited by light availability and start to bloom after stabilization of the water column. Nutrient stress is indicated at the

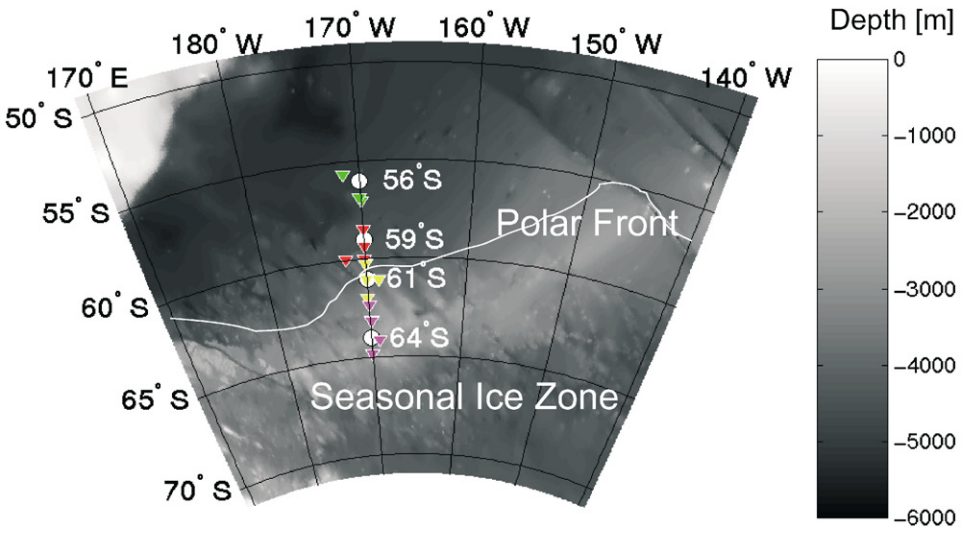

Fig. 1. Southwest Pacific sector of the Southern Ocean. The four model stations along 170°W are indicated (white circles). The locations of the profiles used to restore the simulated temperature and salinity are indicated by the colored triangles. The bathymetry was plotted using the 5 min resolution Navy ETOPO5 data.

end of the growing season, but phytoplankton accumulation rates drop before nutrient stress occurs, implying losses may be due to grazing or sinking (Abbott et al., 2000). There is no evidence for a higher annual production in the vicinity of the PF compared to the PFZ and SIZ (Nelson et al., 2002).

Iron deficiency appears to be an important regulator of primary productivity. Iron enrichment experiments show increased specific growth rates of phytoplankton upon iron addition and a shift in community structure toward larger phytoplankton, namely diatoms (Boyd et al., 2000; Franck et al., 2000; Takeda, 1998; Scharek et al., 1997; de Baar et al., 1995). The higher chlorophyll levels associated with the PF have been suggested to be due to mesoscale upwelling patterns resulting in higher iron supply in the vicinity of the front (de Baar et al., 1995). Iron is thought to exert selective control on phytoplankton by suppressing diatoms more effectively than smaller phytoplankton, while smaller phytoplankton are kept in check by efficient grazing. The coupling between diatoms and mesozooplankton is less tight since mesozooplankton have larger generation timescales. Hence the stimulation of phytoplankton growth by iron inputs due to either natural upwelling or artificial iron enrichment allows an accumulation of diatom biomass while the microzooplankton grazing control is responding quickly enough to prevent small phytoplankton from blooming.

The southwest Pacific sector of the Southern Ocean appears as a variable environment with meridional gradients of light, nutrients and hydrographical properties. Spatially distinct patterns in community structure, primary production, and export are produced by interplaying factors, including light availability and the supply of macro- and micronutrients.

3. Model description

We apply a coupled one-dimensional physical/biological model to four stations spanning the different biogeochemical subsystems in the PFZ, the PF, and the SIZ along 170°W (Fig. 1). The northernmost station at 56°S lies in the PFZ, while the stations at 59°S and 61°S are influenced by the PF. The main axis of the PF jet lies at ~61°S although meanders deviate from the mean path by

more than a degree (Moore et al., 1999a). The southernmost station at 64°S represents the SIZ.

The productivity pattern and community composition change in the different subsystems although the principal components of the ecosystem are the same. Environmental factors that contribute to the functional differences include variations in mixed layer depth, incoming radiation, and nutrient supply. Our aim is to formulate a simple biological model that is able to resolve the environmental controls and the underlying mechanisms that create the latitudinal differences in the functioning of the biological system. By applying the same model with identical parameters at the different locations we want to test the model's ability to capture the different biogeochemical features. A thorough description of the biological model component is given in Section 3.1.

The biological model is coupled to a one-dimensional mixed-layer model such that the evolution of any biochemical scalar C is given by

$$\frac{\partial C}{\partial t} = \frac{\partial}{\partial z}\left(K\frac{\partial C}{\partial z}\right) + \mathrm{sms}(C),$$

where the first term on the right hand side accounts for vertical mixing and the second term represents the biochemical sources minus sinks (sms) of the particular scalar. The vertical diffusion coefficient K accounts for vertical mixing determined by the mixing parameterization of the physical model component and a uniform background diffusion (see Section 3.2). This set up has two main deficiencies: the absence of any advective and mixing transports in the horizontal direction and the lack of sea-ice dynamics. The PFZ and the SIZ are characterized by large meridional transports of heat, freshwater and nutrients. Large surface fluxes of heat and freshwater due to the freezing and melting of sea ice occur in the SIZ. We apply a restoration of the simulated temperature, salinity and inorganic nutrients, described in detail in Section 3.3 to account for these fluxes. The southernmost station at 64°S is ice-covered during part of the simulation. Since the presence of ice significantly affects the albedo, the light attenuation, and the flux of momentum at the sea surface, we modify the wind stress and the incoming light during ice-covered periods. The modifications are described in more detail in Section 3.4.

3.1. The biological model

The biological model contains 7 state variables: two phytoplankton groups, diatoms *dia* and other small phytoplankton *phy*, one group of zooplankton *zoo*, two inorganic nutrient pools, dissolved inorganic nitrogen *din* and silicic acid *sia*, and two detrital pools, detrital nitrogen det_{N} and detrital silica det_{Si} (Table 1). Diatoms should be included as a separate phytoplankton group because they dominate high productivity events in the SIZ (Brzezinski et al., 2001; Fiala et al., 1998; Bathmann et al., 1997; Jochem et al., 1995). Furthermore, they are estimated to account for ~75% of the primary production in the Southern Ocean (Nelson and Trèguer, 1992) and for a large portion of the export flux (Honjo et al., 2000; Honjo, 1990; DeMaster et al., 1992).

Silicic acid required for diatom growth reaches limiting concentrations in summer (Nelson et al., 2001; Franck et al., 2000). This implies that silicic

Table 1
Model state variables

Symbol	Unit	Variable	Background value
din	mmol N m^{-3}	Dissolved inorganic nitrogen	
sia	mmol Si m^{-3}	Silicic acid	
dia	mmol N m^{-3}	Diatoms	$dia_0 = 0.01$ mmol N m^{-3}
phy	mmol N m^{-3}	Small phytoplankton	$phy_0 = 0.01$ mmol N m^{-3}
zoo	mmol N m^{-3}	Zooplankton	$zoo_0 = 0.05$ mmol N m^{-3}
det_N	mmol N m^{-3}	Detrital nitrogen	$det_{N0} = 0.001$ mmol N m^{-3}
det_{Si}	mmol Si m^{-3}	Detrital silicate	$det_{Si0} = 0.001$ mmol Si m^{-3}

acid is at least temporarily regulating primary productivity and that the cycling of silica should be included. Since silica is necessary for diatom growth, but not taken up by any other plankton group in the model, the cycles of nitrogen and silica are connected only by the diatom group (Fig. 2). Both cycles uncouple during diatom blooms due to different remineralization pathways and different decay rates for detrital silica and nitrogen. The differential remineralization is also referred to as the silica pump (Dugdale et al., 1995) and represents a mechanism for the efficient removal of silica from the euphotic zone. The model is designed to capture the silica pump by distinguishing the detrital fractions of nitrogen and silica as separate pools.

The low supply of the micronutrient iron is probably an important factor for the low productivity levels in the Southern Ocean. Depression of phytoplankton growth rates has been demonstrated in in situ iron enrichment experiments (Boyd et al., 2000; de Baar et al., 1995) and in bottle incubations (Franck et al., 2000; Takeda, 1998; Scharek et al., 1997). Low iron levels exert selective pressure on phytoplankton. Consistently in all iron-enrichment experiments, the dominant species of the phytoplankton community have been reported to shift from small size classes toward larger cells, essentially diatoms (summarized in de Baar and Boyd, 2000). Furthermore the Si:N stoichiometry of diatoms is sensitive to iron availability with 2 to 3-fold increased Si:N ratios in iron-stressed diatoms (Takeda, 1998; Hutchins and Bruland, 1998), implying an increased efficiency of the silica pump in the iron-depleted waters of the Southern Ocean. The effect of iron is included implicitly in our model by employing phytoplankton growth parameters typical for the low iron levels and a typical Si:N ratio of 4. That is, we assume a continuously low ambient iron concentration during the simulation period and no significant perturbations due to iron supply that reach levels where phytoplankton growth rates or the diatom stoichiometry are affected. This assumption is consistent with iron measurements during the AESOPS cruises by Measures and Vink (2001), who report low dissolved iron concentrations that vary only in a confined region between 0.1 and 0.35 nM. In a companion paper (Fennel et al., 2003) we investigate the response of the model system to higher iron supply. The model experiments described in that paper required an inclusion of iron and a modification of the formulation of phytoplankton growth.

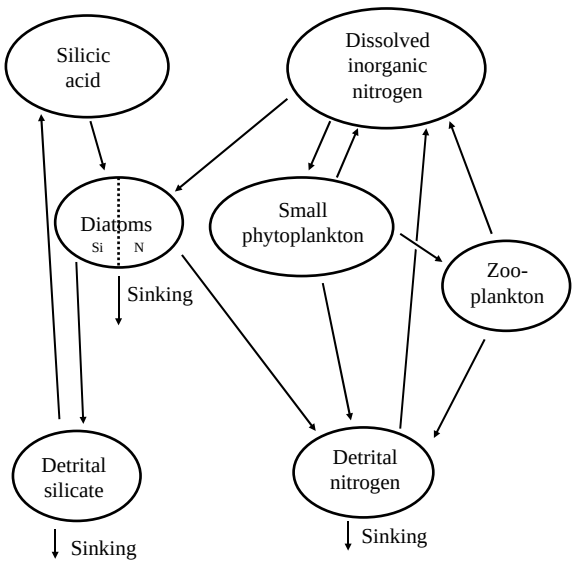

Fig. 2. Schematic of the biological model.

The model includes only one zooplankton group, namely microzooplankton, grazing on the small phytoplankton. The grazing by microzooplankton is an important component of the system providing control on pico- and nanoplankton. The microzooplankton are able to respond quickly to changes in primary production (Becquevort, 1997), and grazing rates between 70 and 80% of phytoplankton productivity have been reported during the AESOPS cruises (Landry et al., 2002), keeping small phytoplankton standing stocks in check. Mesozooplankton grazing on diatoms is not included, since its grazing impact on phytoplankton stocks in the Southern Ocean is generally thought to be small (Urban-Rich et al., 2001; Bathmann et al., 2000; de Baar and Boyd, 2000; Razouls et al., 1998; Dubischar and Bathmann, 1997). A few studies found high grazing rates; e.g., Froneman et al. (2000) report mesozooplankton ingestion rates from 0.14-89% of daily primary production. However, during the AESOPS cruises Urban-Rich et al. (2001) found that

Table 2
Biological model parameters

Symbol	Value	Unit	Parameter
μ_{dia}^{max} ***	0.7	d^{-1}	Maximum growth rate of diatoms
μ_{phy}^{max} **	0.7	d^{-1}	Maximum growth rate of small phytoplankton
k_{Si} *	3.6	mmol Si m^{-3}	Half-saturation concentration for uptake of silicic acid
$\frac{Si}{N}$	4	mol Si : mol N	stoichiometry of diatoms
k_N —	0.5	mmol N m^{-3}	Half-saturation concentration for uptake of DIN
$\bar{\alpha}$ ***	0.3	$(W\ m^{-2})^{-1}$	Ratio of α^B to P_{max}^B in P vs. I curve
$L_{dia,det}$ *	0.2	d^{-1}	Diatom mortality rate
$L_{phy,din}$ —	0.05	d^{-1}	Phytoplankton respiration rate
$L_{phy,det}$ —	0.15	d^{-1}	Phytoplankton mortality rate
w_{dia} **	6	m d^{-1}	Sinking velocity of diatoms
μ_{zoo}^{max} **	0.6	d^{-1}	Maximum grazing rate
I *	12	$(mmol\ N\ m^{-3})^{-2}$	Exponential factor in μ_{zoo}
$L_{zoo,din}$ *	0.05	d^{-1}	Zooplankton respiration rate
$L_{zoo,det}$ *	0.15	d^{-1}	Zooplankton mortality rate
r_N *	0.1	d^{-1}	Remineralization rate of detrital nitrogen
r_{Si} *	0.05	d^{-1}	Remineralization rate of detrital silicon
w_{det} **	10	m d^{-1}	Sinking velocity of detritus

The sensitivity of the model results to perturbations of the parameters is indicated by the asterisks besides the symbols: * * * represents the strongest response; — represents no response of the model to parameter variations of ±50% (see Section 5).

mesozooplankton is not important in regulating phytoplankton growth, in agreement with results from the Atlantic (Dubischar and Bathmann, 1997) and Indian sectors (Razouls et al., 1998). A possible effect on community structure by mesozooplankton grazing on microzooplankton in late spring and summer (Razouls et al., 1998; Perissinotto et al., 2000) is neglected. The role of mesozooplankton as mediators for the vertical transport of biogenic silica and carbon due to fecal pellet production (Dagg et al., 2003) is implicitly accounted for by the sinking of diatoms. Two potential factors contribute to the small grazing loss by mesozooplankton. Firstly, mesozooplankton have much longer generation timescales than the diatoms, hence they are not able to respond quickly to accumulation of diatoms (Jochem et al., 1995; de Baar and Boyd, 2000). Secondly, the morphology of the highly silicified Antarctic diatoms may help to minimize grazing (Verity and Smetacek, 1996).

The dynamics of the ecological state variables are determined by the following set of equations. The corresponding parameter values are given in Table 2. The biological sources and sinks of the diatoms are defined by

$$\mathrm{sms}(dia) = \mu_{dia}(sia, din, E)dia - L_{dia,det}(dia - dia_0) - w_{dia}\frac{\partial}{\partial z}dia. \quad (1)$$

The growth rate of the diatoms μ_{dia} depends on the concentrations of silicic acid *sia*, dissolved inorganic nitrogen *din*, and the photosynthetically available radiation E according to

$$\mu_{dia}(sia, din, E) = \mu_{dia}^{max}(1 - \exp(-\bar{\alpha}E)) \times \min\left(\frac{sia}{k_{Si} + sia}, \frac{din}{k_N + din}\right), \quad (2)$$

where μ_{dia}^{max} is the maximum growth rate and k_{sia} and k_N are the half-saturation constants for the uptake of *sia* and *din*, respectively. We assume that either silicic acid or inorganic nitrogen is limiting

the growth rate following a Michaelis–Menten response, while the other nutrient is taken up in a fixed stoichiometric ratio. The limiting nutrient is determined as the one in shortest supply relative to need according to Liebig's Law of the Minimum.

The photosynthesis-light response $(1-\exp(-\bar{\alpha}E))$ in (2) is based on the equation

$$P^B = P^B_{\max}\left(1-\exp\left(-\frac{\alpha^B E}{P^B_{\max}}\right)\right), \tag{3}$$

suggested by Cullen (1990) to describe the chlorophyll-specific rate of photosynthesis in the water column P^B as function of irradiance E and chlorophyll. $P^B_{\max}$ is the maximum rate of photosynthesis normalized to chlorophyll and α^B is the initial slope of the P^B vs. E curve. This equation is a reformulation of the mechanistic model of Sakshaug et al. (1989) and equivalent to the equation of Platt et al. (1980) if no photoinhibition is assumed. Since growth rates in the model are considered as biomass-specific, the chlorophyll-specific formula (3) was slightly modified before inclusion in Eq. (2). In Eq. (2) the highest growth rate, which is achieved for light- and nutrient-saturated conditions, is determined by the biomass-specific maximum growth rate $\mu^{\max}_{\text{dia}}$ instead of $P^B_{\max}$. Since α^B and $P^B_{\max}$ are not independent in $(1-\exp(-\alpha^B E/P^B_{\max}))$, we replaced their ratio by one parameter $\bar{\alpha} := \alpha^B/P^B_{\max}$.

E represents the fraction of light that is effective in photosynthesis and is exponentially decreasing with water depth according to

$$E(z) = E_0 \cdot \text{par} \cdot \exp(-z(K_w + K_{\text{chl}}\,\text{chl}(z))). \tag{4}$$

z is the water depth, E_0 is the incoming light just below the sea surface, and par is set to 0.43 and represents the fraction of light available for photosynthesis. $K_w = 0.04\ \text{m}^{-1}$ and $K_{\text{chl}} = 0.03\ \text{m}^{-1}\ (\text{mg chl m}^{-3})^{-1}$ are the light attenuation coefficients for water and chlorophyll, respectively. $\text{chl}(z)$ represents the mean chlorophyll concentration above the actual depth z and is determined by integration over the diatom and small phytoplankton chlorophyll concentrations above the actual depth as

$$\text{chl}(z) = \frac{12}{z}\frac{C}{N}\int_0^z \left(\left[\frac{\text{Chl}}{C}\right]_{\text{dia}} dia + \left[\frac{\text{Chl}}{C}\right]_{\text{phy}} phy\right) \text{d}z'. \tag{5}$$

The conversion from $[\text{mmol N m}^{-3}]$ to $[\text{mg chl m}^{-3}]$ was done using a molar C:N ratio of 6.625 (Redfield) and C/Chl ratios of 45 g g^{-1} and 60 g g^{-1} for the diatoms and the small phytoplankton following Chan (1980). Diatom losses are due to mortality and sinking. An offset dia_0 is included in the formulation of the linear mortality term to ensure that the phytoplankton concentration does not drop below the background concentration dia_0 during low productive periods. w_{dia} is the constant sinking velocity.

The sources and sinks of the small phytoplankton are given by

$$\begin{aligned}\text{sms}(phy) = {} & \mu_{\text{phy}}(din, E)phy - \mu_{\text{zoo}}(phy)zoo \\ & - L_{\text{phy,din}}(phy - phy_0) \\ & - L_{\text{phy,det}}(phy - phy_0),\end{aligned} \tag{6}$$

where the phytoplankton growth rate μ_{phy} depends on the concentration of din according to the Michaelis–Menten kinetics and the photosynthetically available light E. The growth rate is given by

$$\mu_{\text{phy}}(din, E) = \mu^{\max}_{\text{phy}}(1-\exp(-\bar{\alpha}E))\frac{din}{k_N + din}, \tag{7}$$

where $\mu^{\max}_{\text{phy}}$ is the maximum growth rate and k_N is the half-saturation constant for the uptake of din. Small phytoplankton loss terms are grazing by zooplankton and linear losses to the dissolved inorganic nitrogen pool and the detrital nitrogen pool accounting for respiration, exudation and mortality of the small phytoplankton. An offset phy_0 is included in the formulation of the linear losses to ensure that the phytoplankton concentration does not drop below the background concentration phy_0.

The zooplankton dynamics are determined by

$$\begin{aligned}\text{sms}(zoo) = {} & \mu_{\text{zoo}}(phy)zoo - L_{\text{zoo,din}}(zoo - zoo_0) \\ & - L_{\text{zoo,det}}(zoo - zoo_0).\end{aligned} \tag{8}$$

The ingestion of small phytoplankton by zooplankton is parameterized by an s-shaped Ivlev

response (Steele and Henderson, 1992)

$$\mu_{zoo}(phy) = \mu_{zoo}^{max}(1 - \exp(-Iphy^2)), \quad (9)$$

where μ_{zoo}^{max} is the maximum grazing rate. Metabolic losses and mortality enter the dissolved inorganic and detrital nitrogen pools at linear rates with the background concentration zoo_0 as offset.

The sources and sinks of the *sia* and *din* pools are written as

$$\mathrm{sms}(sia) = -\frac{\mathrm{Si}}{\mathrm{N}}\mu_{dia}(sia, din, E)dia + r_{Si}det_{Si}, \quad (10)$$

and

$$\begin{aligned}\mathrm{sms}(din) = &-\mu_{dia}(sia, din, E)dia - \mu_{phy}(din, E)phy \\ &+ L_{phy,din}(phy - phy_0) \\ &+ L_{zoo,din}(zoo - zoo_0) + r_N det_N. \end{aligned} \quad (11)$$

Si/N represents the fixed intracellular Si:N ratio of the diatoms and is included to convert from the diatom biomass unit [mmol N m^{-3}] to [mmol Si m^{-3}]. r_{Si} and r_N are the remineralization rates of det_{Si} and det_N, respectively.

The time rates of change of the detrital pools are given as

$$\begin{aligned}\mathrm{sms}(det_{Si}) = &-r_{Si}det_{Si} + \frac{\mathrm{Si}}{\mathrm{N}}L_{dia,det}(dia - dia_0) \\ &- w_{det}\frac{\partial}{\partial z}det_{Si}, \end{aligned} \quad (12)$$

and

$$\begin{aligned}\mathrm{sms}(det_N) = &-r_N det_N + L_{dia,det}(dia - dia_0) \\ &+ L_{phy,det}(phy - phy_0) \\ &+ L_{zoo,det}(zoo - zoo_0) \\ &- w_{det}\frac{\partial}{\partial z}det_N. \end{aligned} \quad (13)$$

w_{det} is the constant sinking velocity of the particulate detrital material.

3.2. Set up of the physical model

The physical component of the coupled model simulates the vertical mixing of temperature, salinity, and the biochemical scalars and the evolution of the mixed-layer depth in response to synoptic surface fluxes of heat and momentum. The mixed-layer model employs the parameterization described by Price et al. (1986) modified by the inclusion of a uniform background diffusion. The turbulent mixing due to surface forcing is given by a Richardson-number dependent parameterization. In the model, mixing occurs to ensure the static stability of the water-column and to satisfy stability criteria of the bulk Richardson-number and the gradient Richardson number. A thorough description is given in Price et al. (1986). In addition to the surface mixing a uniform background diffusion of 1×10^{-6} m^2 s^{-1} was applied to parameterize the turbulent transport below the thermocline.

The model was set up on a uniform grid, covering the upper 400 m of the water column with a 5-m resolution. It was forced with daily values of the wind stress and the sensible, latent and downward short-wave components of the heat flux from the NCEP reanalysis data set. A typical albedo of 0.04 (Payne, 1972) was employed for the short-wave component. The heat penetration of insolation was described by a double exponential depth dependence (Kraus, 1972) that includes a short- and a long-wave component of solar radiation. The attenuation parameters were chosen to represent fairly clear, mid-ocean water (Jerlov water type IA; Jerlov, 1976) in agreement with observations in Subantarctic waters south of New Zealand (Howard-Williams et al., 1995). The daily cycle of solar radiation was calculated from the astronomical formula (Brock, 1981) employing the correction of the solar constant by Duffie and Beckman (1980). The lower boundary of the model is open to allow diffusive fluxes and sinking particles to cross the base of the model.

The model simulation started in October 1997 and was run for two years with the same atmospheric forcing. 1997 forcing fields were used from July to December and 1998 forcing fields from January to June. The initial conditions for temperature and salinity were interpolated from profiles measured at the end of October 1997 during the early spring cruise (Survey I). The biochemical variables were initially set to the constant background values given in Table 1, except for the inorganic nutrients. Dissolved inorganic nitrogen *din* and silicic acid *sia* were initialized with nitrate + ammonium and silicic

acid profiles measured at the end of October 1997 during Survey I. All model results shown in this paper were taken from the second year of the simulation.

3.3. Restoration of temperature, salinity and nutrients

To account for unresolved advective and surface fluxes of temperature and salinity these variables are restored to observed profiles measured during the AESOPS cruises between October 1997 and March 1998. Furthermore, advective fluxes of nutrients are important to replenish the intermediate and surface nutrient levels in winter. We apply a restoration of the inorganic nutrients below 100 m. Nitrate and silicic acid concentrations in the intermediate water appear to be highly correlated with density. For the restoration of nutrients we take advantage of this correlation and restore the model to values predicted by an approximation of nutrient concentrations for the actual density.

For each of the stations, one temperature and salinity profile per month was chosen to cover the period between October 1997 and March 1998. Profiles were considered if they were located within 100 km ($\sim 1^\circ$ latitude) of the model station. The locations of the restoration profiles are indicated on the map in Fig. 1. Due to latitudinal differences in the location of the restoration profiles the temperatures and salinities show an offset of up to 1°C and 0.25 PSU between 200 and 400 m. These differences are not caused by surface fluxes or advection. We attempted to eliminate these deviations for the restoration. For each station we calculated the mean of the temperature and salinity properties over the 200–400 m depth range. Then each profile was corrected by subtracting its deviation from the mean.

Restoration profiles are only available for austral summer. We restore to the AESOPS profiles between October and March with a timescale of 20 days. This procedure gives good agreement between the simulated and observed profiles as shown in the model/data comparison of temperature and salinity for 64°S (Fig. 3). The station at 64°S is ice covered until the second half of November in 1997. Large fluxes of heat and freshwater occur during the melting period. The meltwater input is an important factor for the stabilization of the upper water column, but it is not explicitly resolved in the model. Instead, the fluxes associated with the sea-ice dynamics are induced implicitly by the restoration of temperature and salinity. Fig. 4 shows the ice coverage and the simulated salinity at station 64°S illustrating the freshening of the upper water column during ice melt. From mid November to early December, when the ice coverage is reduced from 60% to 0, the surface salinity decreases from 34.2 to 33.6 PSU and the upper water column stabilizes with mixing depths around 30 m. The simulated mixed-layer depth compares well with estimates obtained from AESOPS profiles (Fig. 5).

The meridional gradients in nitrate and silicic acid concentrations and the meridional transport of water masses described in Section 2 imply a horizontal transport of nutrients that is not explicitly included in the one-dimensional model. Our restoration of the inorganic nutrients below the thermocline assumes that the nutrients are transported along isopycnals. We approximated the nutrient concentrations as function of density by fitting 3rd-order-polynomials to the AESOPS nitrate and silicic acid bottle data. The correlations are highly significant, confirming that our assumption is consistent with the observations. The significance of the approximation is illustrated in Fig. 6, which shows the data and their polynomial approximations with 95% confidence intervals. The polynomial approximations were calculated for nitrate and silicic-acid bottle data for each model station and used to restore the *din* and *sia* concentrations below 100 m depth (Fig. 6).

3.4. Modification of light and wind stress due to sea ice

The presence of ice significantly affects the fluxes of light and momentum at the sea surface. Ice cover reduces the incoming light just below the sea surface by increased albedo and high light attenuation within the ice sheet. The transfer of momentum at the sea surface is influenced by ice

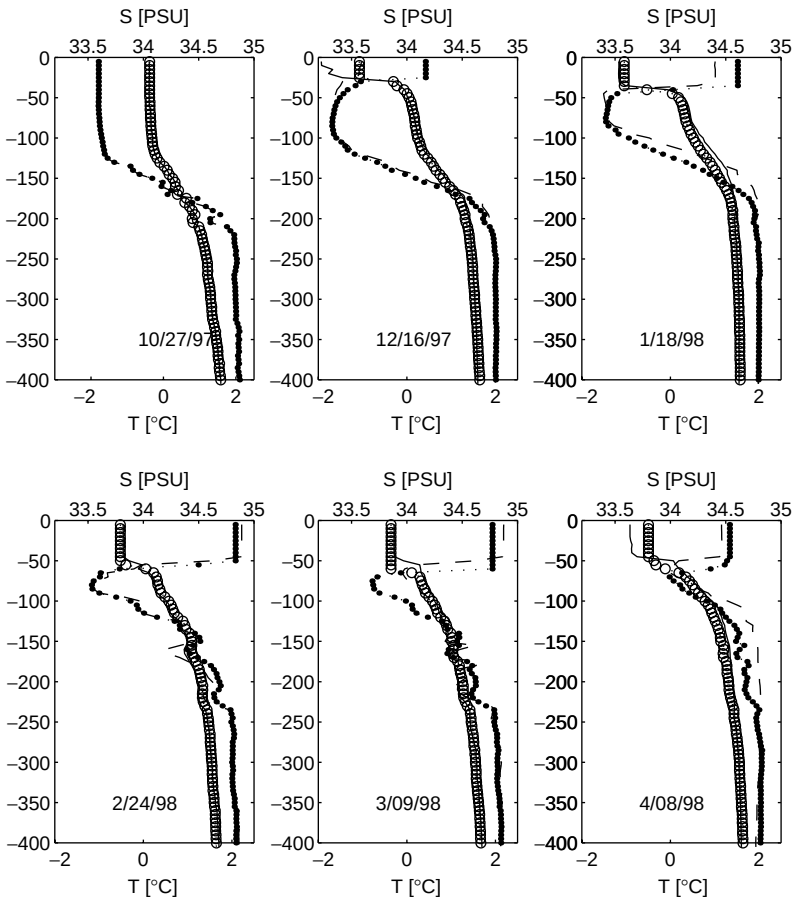

Fig. 3. Comparison of simulated temperature and salinity with the restoration profiles at 64°S. Salinity is represented by open circles (model) and the solid line (restoration profiles). Temperature is represented by filled dots (model) and the dashed line (restoration profiles).

because wind speed and drag coefficients are affected.

During ice-covered periods we determine the incoming light just below the sea surface, E_0, as

$$E_0 = E_{\text{top}}(1 - \text{alb}_{\text{ice}}) \exp(-k_{\text{ice}} h), \quad (14)$$

taking into account the increased albedo and the light attenuation within the ice sheet. E_{top} represents the incoming light just above the air–ice interface, alb_{ice} and k_{ice} are the albedo and the attenuation coefficient for ice, respectively, and h is the thickness of the ice sheet. Albedos and extinction coefficients vary greatly for various types of ice and snow (Grenfell and Maykut, 1977). We have chosen an albedo of 0.32, which is a typical value for melting first-year ice, and an extinction coefficient of 0.8, which is an average value for ice without snow (Grenfell and Maykut, 1977). The sea ice is generally between 1 and 2 m thick (Bathmann et al., 2000). We have chosen a thickness of 1 m.

Since sea ice significantly affects wind speed and drag coefficients (Guest et al., 1995 and references therein), the assumption of a spatially homogeneous wind stress is not realistic. In a realistic scenario the wind stress is substantially reduced over pack ice compared to the open ocean. Guest et al. (1995) report a reduction by at least 60% (factor of 0.4) for moderate off-ice winds. We employ this reduction for ice coverage of 90% and

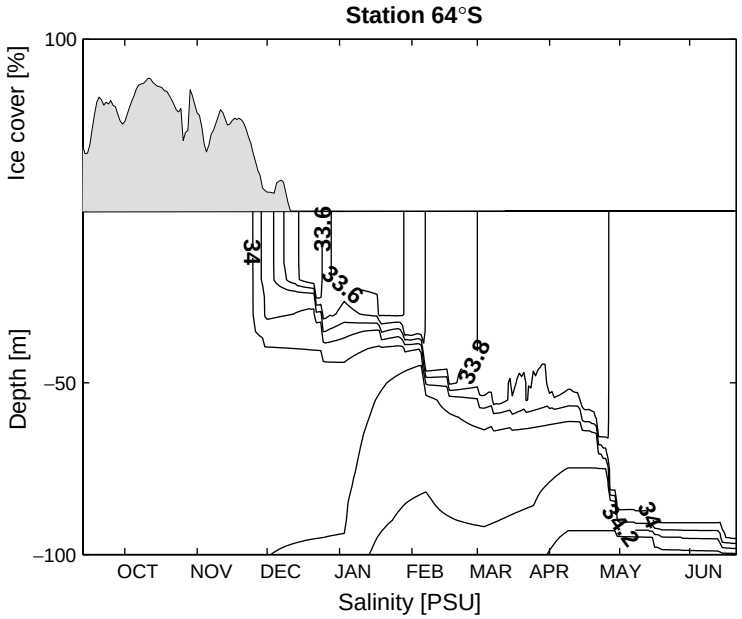

Fig. 4. Ice coverage and simulated salinity at the station at 64°S.

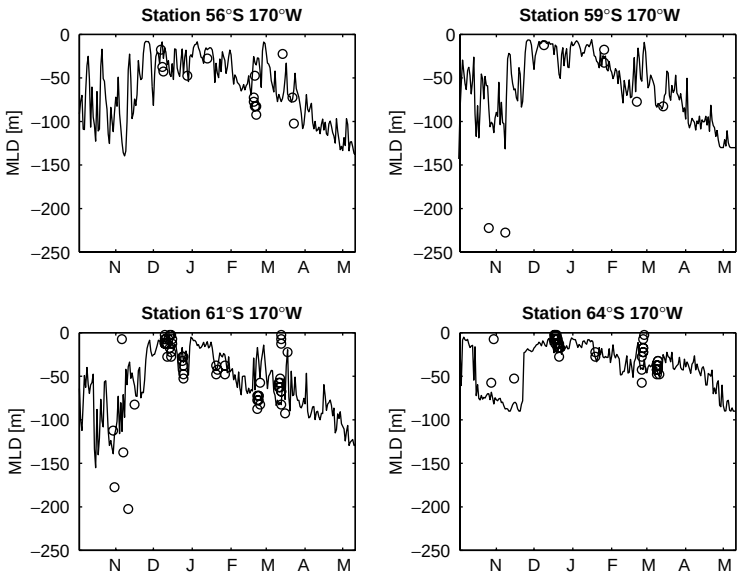

Fig. 5. Simulated daily mean mixed layer depth (MLD; solid line) and MLD estimates (open circles) obtained from AESOPS temperature and salinity profiles. The depth of the mixed layer is defined to be where the gradient of σ_t exceeds 1×10^{-3} kg m^{-4}.

more and determine the wind stress during ice-covered periods, τ_{ice}, as

$$\tau_{ice} = \tau_{ocean}(0.7 - 0.3 \tanh(4(c - 0.4)), \quad (15)$$

where τ_{ocean} is the wind stress over the open ocean and $c \in [0, 1]$ is the fractional ice cover. We use the ice data from the National Snow and Ice Data Center (NSIDC) at the University of Colorado,

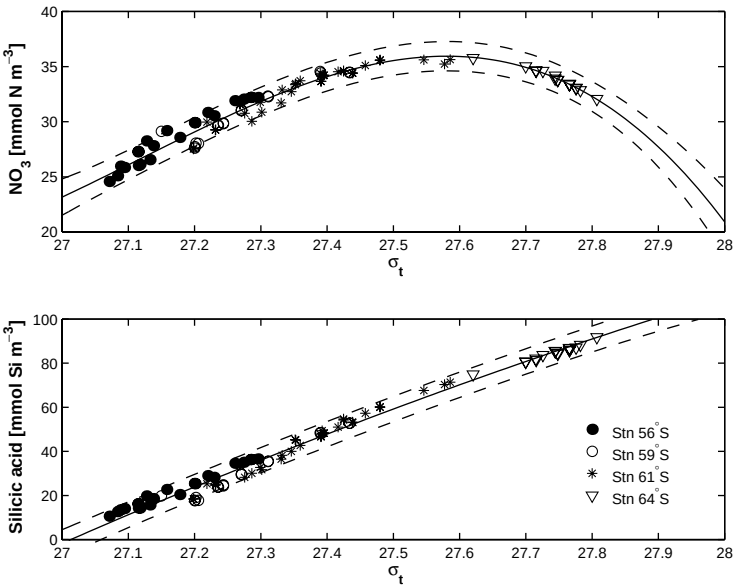

Fig. 6. Polynomial approximations (solid lines) for nitrate (upper panel) and silicic acid (lower panel) as function of density and 95% confidence intervals (dashed lines). The symbols represent AESOPS bottle data from the 200–500 m depth range.

Table 3
Observed phytoplankton growth rates for Antarctic diatom cultures and natural communities

	Growth rate (d^{-1})	Reference
Diatom cultures from the Southern Ocean		
Chaetoceros sp.	0.4–0.7	Jacques (1983)
Fragilariopsis kerguelensis	0.25–0.48	Jacques (1983)
Nitzschia turgiduloides	0.45–0.54	Jacques (1983)
Natural communities		
Southern Ocean	0.4–0.6	Jacques and Minas (1981)
Subantarctic Zone	0.53	Banse (1996)
Polar Frontal Zone	0.4–0.45	Boyd et al. (2000)
Ross Sea	0.1–0.5	Wilson et al. (1986)
Ross Sea	0.04–1.0	Smith et al. (1999)
Weddell Sea	0.5–0.9	El-Sayed and Taguchi (1981)

Boulder, which was processed by J. Keith Moore (Oregon State University) and is available from the US JGOFS data inventory.

3.5. Biological model parameters

Our choices of the biological model parameters, which are usually poorly constrained quantities, are based on observations where available. A few rate estimates, relating to the nutrient uptake and primary production parameters in our model, exist for the study area and other regions in the Southern Ocean. Poorly known are parameters for the metabolical losses and grazing. In this section we summarize available parameter estimates from observations in comparison with our model parameters.

Growth rates reported for cultures of Antarctic diatoms and natural Antarctic communities range between 0.25 and 0.9 d^{-1} (Table 3). In our model

Table 4
Observed photosynthesis-light parameters for Antarctic diatom cultures and natural communities

	P^B_{max}	α^B	$\bar{\alpha}$	Reference
Diatom cultures from the Southern Ocean				
Chaetoceros sp.	1.4	0.2	0.6	Jacques (1983)
Nitzschia turgiduloides	1.1	0.07	0.3	Jacques (1983)
Natural communities				
Southern Ocean	1.2–3.5			Jacques and Minas (1981)
Subantarctic Zone	1.4–1.9	0.04–0.09	0.1–0.2	Dower and Lucas (1993)
Indian Antarctic sector	0.5–5.2	0.07–0.37	0.3–0.6	Jacques (1983)
Weddell Sea	1.0–2.3			El-Sayed and Taguchi (1981)
Weddell Sea	1.9 ± 0.8	0.06 ± 0.02	0.1	Figueiras et al. (1994)

P^B_{max} in [mg C(mg chl)$^{-1}$ h^{-1}] and α^B in [mg C(mg chl)$^{-1}$ h^{-1} μmol m^{-2} s^{-1})$^{-1}$]. $\bar{\alpha}$, the ratio of α^B and P^B_{max}, is converted to [(W m^{-2})$^{-1}$] according to Cullen (1990) (1(μmol m^{-2} s^{-1})$^{-1}$ = 4.15(W m^{-2})$^{-1}$).

Table 5
Observed Si uptake parameters for Antarctic diatom cultures and natural communities. The half-saturation concentration k_{Si} and the maximum uptake rate V_{max} are given in [mmol Si m^{-3}] and [d^{-1}], respectively

	k_{Si}	V_{max}	Reference
Diatom cultures from the Southern Ocean			
Fragilariopsis kerguelensis	12	0.5	Jacques (1983)
Nitzschia turgiduloides	12–22	0.95	Jacques (1983)
Thalassiosira antarctica	4.2	0.54	Sommer (1986)
Corethron criophilum	60.1	0.39	Sommer (1986)
Natural communities in the Southern Ocean			
Pacific sector	2.5–10.5	0.08–0.35	Valerie Franck, pers. comm.
Pacific sector	<1–> 50	0.1–0.3	Nelson et al. (2001)
Ross Sea	2–5		Nelson and Trèguer (1992)
Natural communities outside the Southern Ocean			
	0.4–5.0		Summarized in Nelson and Dortch (1996)

the maximum growth rate for diatoms μ^{max}_{dia} and the maximum growth rate of the small phytoplankton are set to 0.7 d^{-1}. The ratio of reported values of α^B and P^B_{max}, which corresponds to $\bar{\alpha}$ in our model, varies between 0.1 and 0.6 (W m^{-2})$^{-1}$ for cultures and natural assemblages of phytoplankton. In the model $\bar{\alpha}$ is set to 0.3 (W m^{-2})$^{-1}$ (Table 4). The parameters for light attenuation due to water and chlorophyll are set to 0.04 m^{-1} and 0.03 m^{-1}(mg chl m^{-3})$^{-1}$ for K_w and K_{chl}, respectively, and are consistent with the attenuation parameters reported by Howard-Williams et al. (1995).

The half-saturation concentration for the uptake of dissolved inorganic nitrogen k_N is set to 0.5 mmol N m^{-3}, a value adapted from Pondaven et al. (1998). The half-saturation concentration for the uptake of silicic acid is known to be high for diatoms from the Southern Ocean compared to other regions (Table 5), but extreme variations of two orders of magnitude have been reported for the Pacific sector of the PF region (Nelson et al., 2001). The choice of k_{Si} is further complicated by the fact that the half-saturation concentration for uptake of silicic acid is a poor measure for the half-saturation concentration for actual diatom growth (Nelson et al., 2001). Diatoms are relatively flexible in their intracellular Si:N ratio, and near-maximum cell division rates can be sustained even when ambient concentrations of silicic acid limit Si uptake by diminishing the cellular Si content (Sullivan, 1986). Hence Si uptake rates may appear

to be limited by ambient silicic acid concentrations, but this does not necessarily imply limitation of growth. The half-saturation concentration for diatom growth is expected to be much lower than the unusually high values for uptake found in the Southern Ocean (Nelson and Dortch, 1996), particularly at the high levels of ambient silicic acid. The cellular Si:N ratio for the diatoms in our model is assumed to be constant. Since no changes in the intracellular stoichiometries are allowed, nutrient uptake and growth are directly coupled in the model. Hence our choice of k_{Si} should conceptually represent the half-saturation value of growth rather than uptake. Nelson and Dortch (1996) summarize studies comparing Si-uptake and growth parameters for diatoms and conclude that the half-saturation of growth is usually only 10–20% of the half-saturation of uptake. Assuming a value of 15%, the above-mentioned range of half-saturation constants for Si-uptake from ~ 0 to ~ 50 mmol Si m^{-3} (Nelson et al., 2001) is reduced to 0 to 7.5 mmol Si m^{-3}. Furthermore, most of the values determined by Nelson et al. (2001) lie in the lower half of the interval. Consistent with these observations, we set the parameter k_{Si} to 3.6 mmol Si m^{-3}.

The Si:N stoichiometry of cultured diatoms under iron-depleted conditions ranges from 2.3 to 3 mol Si:mol N (Takeda, 1998; Hutchins and Bruland, 1998). In the Southern Ocean, Si:N ratios of up to 6 mol Si:mol N have been found (Brzezinski et al., 2001; Jacques, 1983) and an Si:N disappearance ratio of 4.5 mol Si:mol N in Antarctic surface waters has been observed by Minas and Minas (1992). In agreement with these values, we use a Si:N stoichiomety of 4.

The sinking rates of diatoms and detritus are important parameters since the simulated export flux depends directly on their choice. Estimated in situ and observed in vitro sinking rates vary enormously. Maximum sinking rates of individual diatom cells are generally well below 2 m d^{-1} (Bienfang, 1980, 1981; Bienfang et al., 1982; Muggli et al., 1996), but episodic mass sedimentation events of cell aggregates with greatly accelerated sinking rates occur in senescent diatom blooms upon nutrient depletion (Smetacek, 1985). Sinking rate estimates for the aggregates, which consist of small particles and intact cells are 40 m d^{-1} (Smetacek 1984), > 70 m d^{-1} (Platt et al., 1983), and > 100 m d^{-1} (Alldredge and Gottschalk, 1989). The second main vehicle for rapid vertical particle export besides aggregates are fecal pellets. An extremely high sinking rate of > 1000 m d^{-1} has been reported for the fecal pellets of salps (Bruland and Silver, 1981). In our model, the sinking rates for diatoms w_{dia} and the detrital pools w_{det} are set to 6 and 10 m d^{-1}, respectively.

Estimates of the specific dissolution rate of biogenic silica in the Southern Ocean by Trèguer et al. (1989) range from 0.007 to 0.048 d^{-1}. Nelson and Gordon (1982) report values between 0.01 and 0.045 d^{-1}, and Brzezinski et al. (2001) observed values between 0.032 and 0.089 d^{-1} in the southwest Pacific sector. We chose a value of 0.05 d^{-1} for the remineralization rate of detrital silica. The remineralization rate of detrital nitrogen in the model is set to 0.1 d^{-1}, following Pondaven et al. (1998).

4. Model results in comparison with observations

4.1. Chlorophyll

The changes in chlorophyll as a function of latitude are captured in our simulations at the four model stations (Figs. 7 and 8). North of the PF, chlorophyll levels are low throughout the year with little seasonal change and low summer values (Banse, 1996). Mean surface chlorophyll concentrations are typically $< 0.3 - 0.4$ mg m^{-3} (Moore et al., 2000). In agreement with the observations, the simulated maximum values of chlorophyll at 56°S are low with maximum values of 0.5 mg chl m^{-3} during summer (Figs. 7 and 8).

In the vicinity of the PF chlorophyll levels are higher. This is thought to be due to the high mesoscale variability of the frontal region, which generates favorable conditions for phytoplankton growth (Barth et al., 2001; Moore et al., 1999b). The model station at 61°S stands for the PF regime, and peak chlorophyll concentrations of ~ 1 mg m^{-3} are predicted at this site. At 61°S, the simulated mixed layer in summer is temporarily

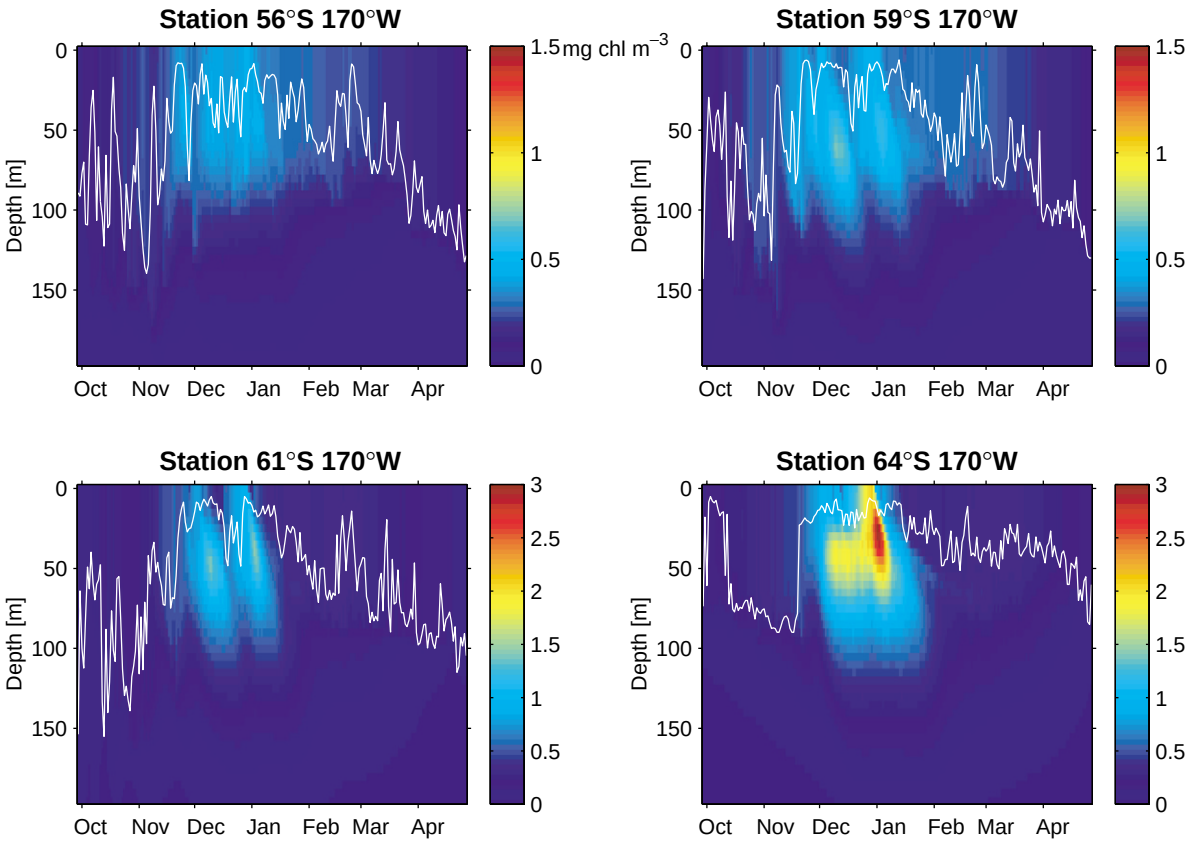

Fig. 7. Simulated chlorophyll concentrations between October 1997 and April 1998 at the four model stations. The daily mean of the simulated mixed layer depth (white line) is plotted as well. The chlorophyll concentration is calculated assuming a C:N ratio of 6.625 and C:chl ratios of 45 and 60 for the diatoms and the small phytoplankton, respectively.

shallow with depths between 10 to 20 m in contrast to the model station at 56°S where the mixed layer depth fluctuates around ~40 m (Fig. 7). The variation in mixed-layer depth is one of the main differences between the northernmost station and the PF station in our simulation and contributes to the higher chlorophyll levels in the vicinity of the PF. Interestingly we do not need to invoke an increased upwelling of iron as suggested by de Baar et al. (1995) to stimulate the higher productivity in the frontal region.

The highest chlorophyll concentrations of up to 2 mg m^{-3} are simulated at the southernmost station at 64°S (Figs. 7 and 8), where an intense diatom bloom was observed after the retreat of the ice-edge (Brzezinski et al., 2001). The magnitude and the temporal course of the simulated values compare well with the data (Fig. 8). The mixing regime at this station is different when compared to the three northern stations. The mixed layer is shallower, with depths around 15 m, and stratification is more pronounced due to the input of fresh meltwater in spring.

4.2. Nutrients

The simulated course of the surface nutrient concentrations in comparison with the corresponding observed values is shown in Fig. 9. At all stations the model results compare well with the observed magnitude and temporal course of the inorganic nutrients. Also the mean nutrient concentrations in the upper 150 m of the water column agree well (Fig. 10).

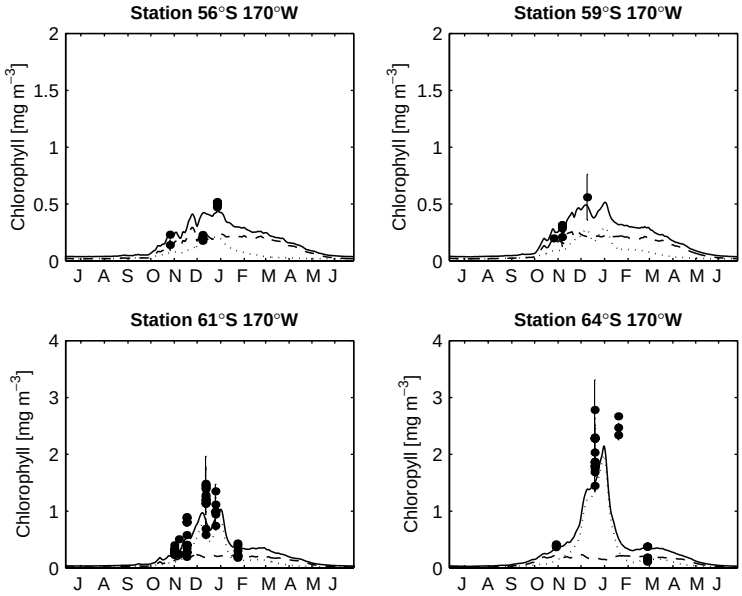

Fig. 8. Comparison of simulated and observed surface chlorophyll concentrations at the four model stations. The solid line represents the total simulated chlorophyll, while the dashed and dotted lines represent the simulated chlorophyll of small phytoplankton and diatoms, respectively. Each filled circle represents the mean surface value of a measured chlorophyll profile. Surface values are obtained by vertical integration over the uppermost 60 m.

At the northernmost station, the measured surface DIN concentrations decrease only slightly from 25 mmol N m^{-3} in late October to 20 mmol N m^{-3} in late February. The corresponding uptake of silicic acid is more pronounced with a reduction of surface concentrations from 14 mmol Si m^{-3} to 3 mmol Si m^{-3}. The minimum simulated silicic acid concentration of 3 mmol Si m^{-3} is close to the half-saturation concentration k_{Si} of 3.6 mmol Si m^{-3}, implying that silicic acid is at least temporarily regulating diatom productivity at this site.

In the vicinity of the PF at 61°S, a seasonal reduction of DIN from $\sim$30 mmol N m^{-3} to $\sim$20 mmol N m^{-3} occurs (Fig. 9). Silicic acid is reduced from $\sim$30 to $\sim$4 mmol Si m^{-3}. The seasonal reduction of DIN and the drawdown of silicic acid at this site are roughly doubled compared to the nutrient reduction at 56°S. The measured nutrient concentrations at 61°S are scattered and reflect the high variability associated with the meandering front, but the simulated nutrients lie within the range of the measured data.

At the southernmost station at 64°S, the strongest reduction of surface concentrations is found. Observed DIN decreases from $\sim$30 mmol N m^{-3} to $\sim$20 mmol N m^{-3}, and observed silicic acid decreases from a maximum value of $\sim$50 mmol Si m^{-3} to a minimum of $\sim$4 mmol Si m^{-3}, indicating the increasing importance of diatoms.

Comparing the seasonal reduction of surface nutrients at the four stations, there is a dramatic southward increase in the drawdown of silicic acid, while the seasonal drawdown of DIN increases only slightly. This indicates the uncoupling of the nitrogen and silica cycles and the growing importance of the silica pump toward the south. The differences in light conditions between the stations influence the pace at which silicic acid is taken up. At the northernmost station, where the mixed layer depths are larger, a drawdown of 10 mmol Si m^{-3} takes more than two months (from late October until mid January) while at the southernmost station about 45 mmol Si m^{-3} are taken up in about 1 month (December).

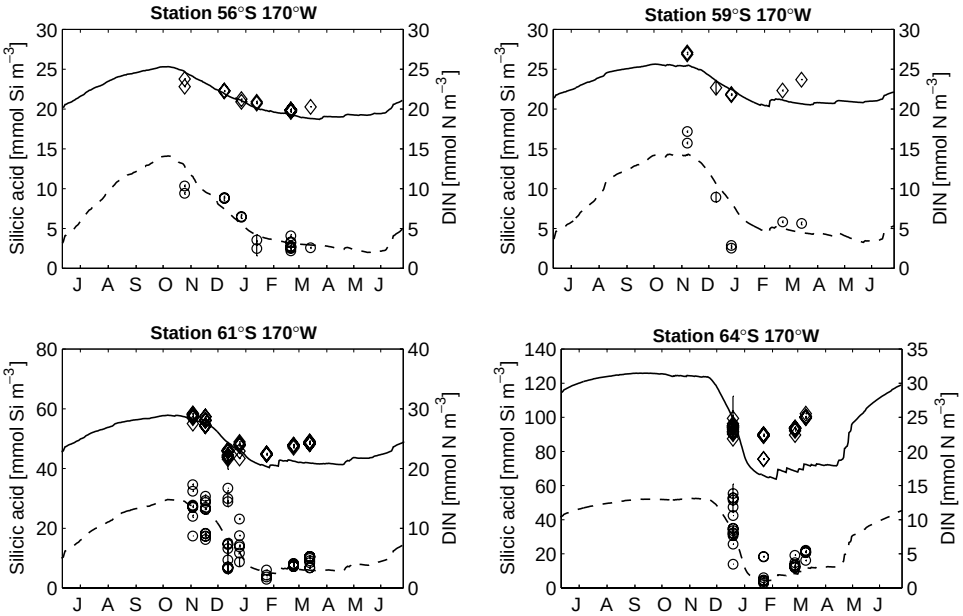

Fig. 9. Comparison of simulated and observed surface nutrients at the four model stations. Silicic acid concentrations are represented by the dashed line (model) and the open circles (data). Dissolved inorganic nitrogen ($NO_3 + NH_4$) values are represented by the diamonds (data) and the solid line (model). Surface nutrient values were obtained by vertical integration over the uppermost 50 m at the two northern stations and over the uppermost 30 m at the two southern stations.

4.3. Community structure

In the Southern Ocean, phytoplankton blooms are generally dominated by larger phytoplankton (> 20 μm), mainly diatoms (de Baar and Boyd, 2000; Fiala et al., 1998; Jochem et al., 1995; Laubscher et al., 1993). These periods of high productivity represent deviations from the recycling system, which is otherwise present and characterized by low but stable standing stocks of small plankton size classes (de Baar and Boyd, 2000) and intense microzooplankton grazing (Landry et al., 2002; Becquevort, 1997). Furthermore a spatial distinction of the phytoplankton community structure is observed with nanoflagellates dominating north and diatoms dominating south of the PF (Mengelt et al., 2001).

This qualitative picture is captured by the model (Fig. 11). North of the PF, the diatom biomass (at maximum 0.1 mmol N m^{-3}) is lower than the small phytoplankton biomass at around 0.2 mmol N m^{-3}. Zooplankton biomass is in the same range as phytoplankton at this site. At the PF station at 61°S, a diatom bloom occurs with a maximum biomass of 0.5 mmol N m^{-3}. The small phytoplankton are effectively controlled by zooplankton grazing and do not exceed concentrations of ~0.2 mmol N m^{-3}. The zooplankton biomass varies around 0.3 mmol N m^{-3}. At the southernmost station at 64°S, the most intense diatom bloom is simulated with maximum concentrations of 1.3 mmol N m^{-3}.

The biomass of small phytoplankton and zooplankton does not show a marked spatial pattern between the different locations. Small phytoplankton and zooplankton biomass remains low and relatively stable at all four stations. A pronounced spatial pattern is found in diatom abundance, which is low at the northernmost station but increases dramatically toward the south. A comparison of simulated and observed biogenic silica concentrations (Fig. 12) gives a quantitative confirmation of this spatial pattern. The data for the northern stations at 56°S and 59°S are sparse, but suggest significantly lower biogenic silica concentrations than at 61°S and

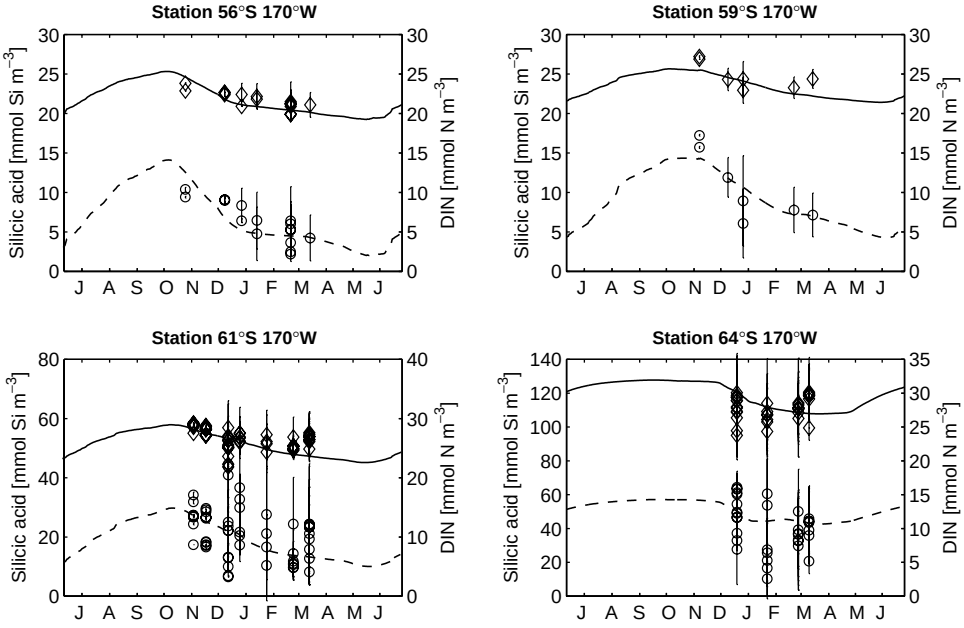

Fig. 10. Same as Fig. 9, but nutrients are integrated over the upper 150 m.

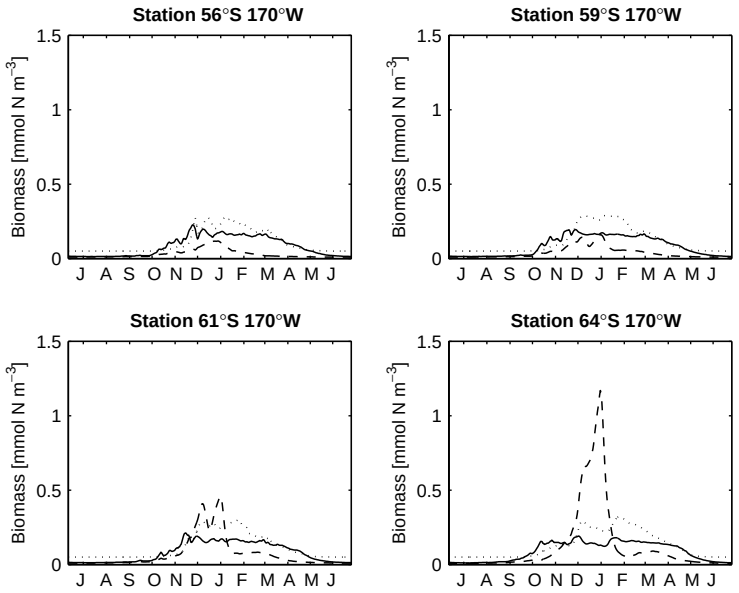

Fig. 11. Simulated biomass of diatoms (dashed), small phytoplankton (solid), and zooplankton (dotted).

64°S, in agreement with the simulated values. At 61°S, the simulated biogenic silica concentrations underestimate the observed values. In the SIZ at 64°S, the observed and simulated values agree well.

4.4. Primary productivity, grazing pressure and vertical flux

During summer, the simulated primary productivity at 56°S ranges between 5 and

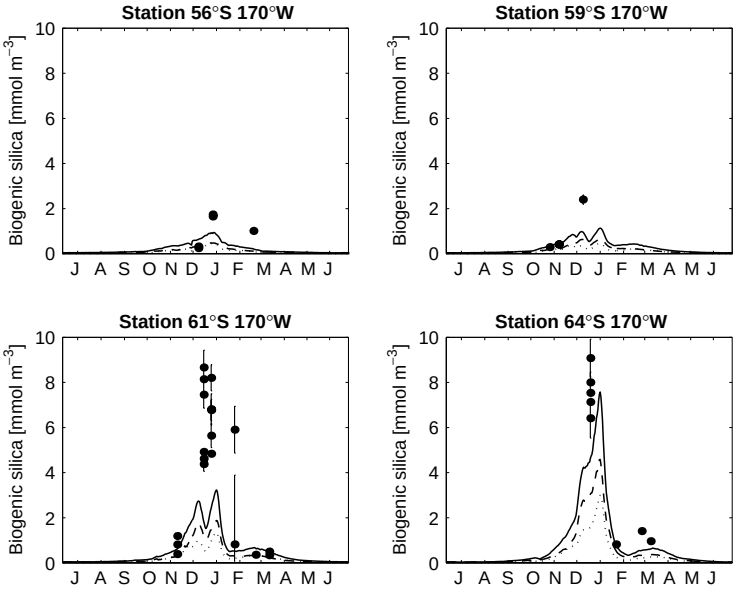

Fig. 12. Comparison of simulated and observed surface concentrations of biogenic silica at the four model stations. The solid line represents the total simulated biogenic silica, while the dashed and dotted lines represent the simulated diatom biomass and detrital silica, respectively. Observations are given as filled circles. Surface values are obtained by vertical integration over the uppermost 60 m.

10 mmol N m^{-2} d^{-1} (Fig. 13). The major fraction of primary productivity is due to small phytoplankton at this station, which make up about 80% of the daily production. At 61°S the simulated primary productivity is higher with values between 10 and 15 mmol N m^{-2} d^{-1} and the contribution of diatoms to the total productivity is higher. At the SIZ station at 64°S, the total productivity ranges between 15 and 30 mmol N m^{-2} d^{-1} during the bloom and only 20 to 30% is due to small phytoplankton (Fig. 13). The magnitude and the latitudinal differences are in agreement with the observations. Sambrotto and Mace (2000) reported daily DIN uptake rates between 10 and 30 mmol N m^{-2} d^{-1} during the AESOPS cruises and observed generally higher uptake of nitrate south of the PF.

Satellite-derived estimates of monthly mean primary productivity (Arrigo et al., 1998) are shown in comparison with the simulated values at the northernmost and the southernmost stations (Fig. 13). The values compare well during the growing season, except for a temporal shift of the high productivity period at 64°S. This time lag between increasing productivity in the satellite-based estimates and in the model can be attributed to the fact the satellite estimates integrate over a relatively large latitudinal band and hence do not capture the exact timing of the bloom at the model location, which is constrained by the retreat of the ice-edge. The order of magnitude of the estimated and simulated yearly integrated production agrees well (Table 6). In our simulation, the contribution of small phytoplankton reduces toward the south and the diatom production becomes more important.

Our model does not include mesozooplankton grazing on diatoms. This is consistent with observations made during the AESOPS cruises by Landry et al. (2002) who report small grazing losses due to mesozooplankton. Also in other regions of the Southern Ocean, mesozooplankton grazing has been found to be negligible (Razouls et al., 1998; Dubischar and Bathmann, 1997). On the other hand, microzooplankton grazing is observed to be intense and responds rapidly to increases in primary production (Landry et al., 2002; Becquevort, 1997). Landry et al. (2002)

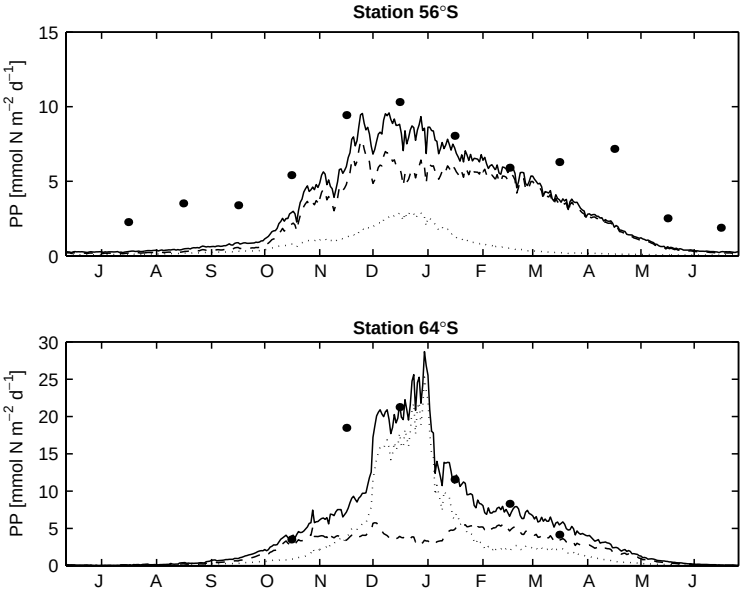

Fig. 13. Comparison of simulated and estimated daily primary productivity. The solid line represents total productivity while the dotted and dashed lines represent the fractions due to diatoms and small phytoplankton, respectively. The filled dots represent corresponding monthly means of primary productivity estimated from CZCS satellite data (Arrigo et al., 1998).

Table 6
Yearly integrated values of simulated primary productivity in comparison with observation-based estimates

	56°S170°W	59°S170°W	61°S170°W	64°S170°W
Total DIN uptake [*mol N m*$^{-2}$ *yr*$^{-1}$]				
Model	1.0	1.2	1.4	1.8
^{18}O production	2.4		1.8	2.3
^{14}C uptake	1.0		1.3	1.3
CZCS estimates	2.0			2.0
Total Si uptake [*mol Si m*$^{-2}$ *yr*$^{-1}$]				
Model	0.21	0.34	0.7	1.1
^{32}Si uptake	0.76		1.9	3.0
DIN uptake of small phytoplankton (% *of total uptake*)				
Model	80%	73%	56%	43%
DIN uptake of diatoms (% *of total uptake*)				
Model	20%	27%	44%	57%
Grazing pressure (% *of phy production*)				
Model	40%	42%	42%	45%

Values for ^{18}O production, ^{14}C uptake, and ^{32}Si uptake were taken from Nelson et al. (2002). CZCS estimates are from Arrigo et al. (1998). The fractions of simulated uptake by diatoms and small phytoplankton and the ingestion by zooplankton are given as well.

report losses between 70 to 80% of daily primary production due to microzooplankton grazing. In our simulation daily values of grazing fluctuate between 50 and 100% of small phytoplankton production during summer. The yearly integrated values (Table 6) are lower with grazing of ~40% of small phytoplankton production.

Simulated and observed vertical particle fluxes are shown in Table 7 and Fig. 14. Vertical flux measurements based on sediment traps were

Table 7
Simulated and observed vertical particle fluxes

	56°S170°W	59°S170°W	61°S170°W	64°S170°W
Simulated flux of det_{Si} [*mol Si* m^{-2} yr^{-1}]				
At 100 m	0.66	1.10	2.11	3.53
At 400 m	0.19	0.31	0.57	0.89
Estimated flux of biogenic silica [*mol Si* m^{-2} yr^{-1}]				
At 100 m[a]	0.64		1.4	1.4
At 1000 m[b]	0.28		0.38	0.94
Simulated flux of det_N [*mol N* m^{-2} yr^{-1}]				
At 100 m	0.48	0.58	0.76	1.04
At 400 m	0.03	0.04	0.05	0.06
Estimated flux of particulate nitrogen [*mol N* m^{-2} yr^{-1}]				
At 100 m[a]	0.38		0.35	0.41
At 1000 m[b]	0.026		0.026	0.031
Si:N ratio of simulated vertical flux [*mol* : *mol*]				
At 100 m	1.37	1.88	2.78	3.41
At 400 m	5.82	8.10	11.35	14.31
Si:N *ratio of estimated particulate flux* [*mol* : *mol*]				
At 100 m[a]	1.7		4.0	3.4
At 1000 m[b]	10.8		14.6	30.3

Simulated values represent means over the period from October 1997 to September 1998. Flux estimates from Nelson et al. (2002).
[a] Based on ^{234}Th deficits.
[b] Sediment trap data.

obtained within the AESOPS study for the period from December 1997 to January 1998 in the different hydrographical zones (Honjo et al., 2000). Before comparing the observed and simulated vertical particle fluxes in Fig. 14, it should be noted that the values represent different depths with the most shallow traps deployed at ~1000 m and the model extending only to 400 m. Hence only the order of magnitude and the spatial and temporal patterns should be compared. The temporal course of the observed and simulated fluxes agrees well.

The nitrogen fraction of the observed mean vertical POM flux is relatively uniform in the latitudinal direction, while the silica fraction increases significantly southwards at 100 and 1000 m depth (Table 7). The simulated fluxes at 100 and 400 m depth show the same pattern, with a relatively uniform flux of detrital nitrogen at all stations and southward increasing fluxes of detrital silica. The Si:N ratios of the simulated and estimated vertical fluxes consistently show an increase southward due to the increasing importance of diatoms and with depth due to the differential remineralization of nitrogen and silica.

5. Sensitivity of the model results to parameter choices

Defining the parameters in marine ecosystem models is generally not straightforward. In Section 3.5 we summarized the available observation-based estimates for the model parameters in comparison with our parameter choices. Information on metabolical loss rates and grazing is very limited. For parameters related to nutrient uptake, sinking and remineralization, the range of reported values can be substantial. For example, for the half-saturation concentration k_{Si} and the vertical sinking rates w_{dia} and w_{det}, the reported values vary by orders of magnitude. We performed a sensitivity analysis to check how strongly the model results depend on perturbations of the uncertain parameters.

We explored the sensitivity to variations of the parameters by perturbing every parameter by $\pm 50\%$ of its value. Following Pondaven et al. (2000), we explored the effect of the perturbations by comparing selected model outputs. We chose the yearly primary productivity, the vertical particle flux of detritus at 400 m, the maximum

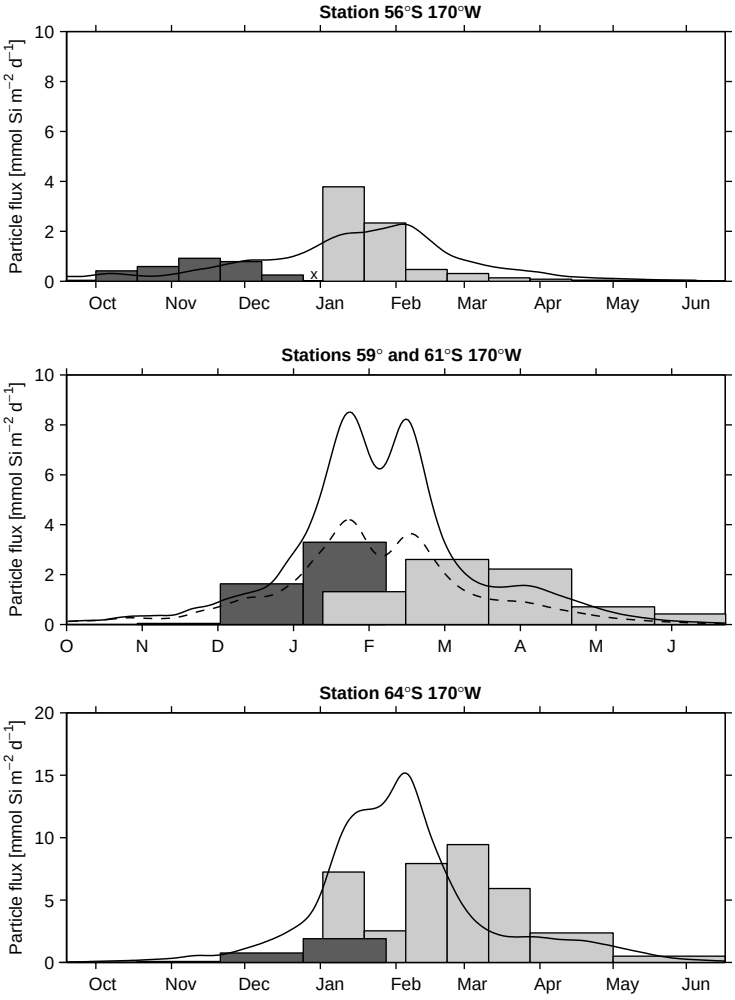

Fig. 14. Comparison of simulated and observed vertical silica fluxes. The lines represent the simulated flux at 400 m, while the bars represent trap data from ~1000 m depth. The dashed line in the middle panel represents the simulated flux at station 59°S, the solid line refers to station 61°S. The trap locations are MS-2 (56°5'S), MS-3 (60°2'S) and MS-4 (63°1'S) from the top to the bottom panel (compare Honjo et al., 2000). Since trap data are missing after January 1998, data from 1997 are plotted as substitutes for 1998 (light gray bars). The cross in the uppermost panel indicates missing data.

concentrations of the three plankton groups *dia*, *phy* and *zoo*, and the minimum concentrations of the inorganic nutrients, *din* and *sia*, as model diagnostics. The model's sensitivity to each of the parameters is indicated in Table 2.

Perturbing the growth and grazing rates μ_{dia}, μ_{phy}, and μ_{zoo} and the light parameter $\bar{\alpha}$ has the strongest effect on the model results. Perturbation of the sinking velocity influenced the simulated export flux markedly. The response of the model to perturbations of the maximum diatom growth rate μ_{dia}^{max} is shown in Fig. 15. The maximum values of the diatom biomass increase almost linearly with increasing μ_{dia}^{max} and roughly double for an increase of μ_{dia}^{max} of 50% (Fig. 15a). The same response is found for the integrated primary productivity and the export flux (Fig. 15c and d). Perturbation of μ_{dia}^{max} has no significant effect on the small phytoplankton and zooplankton biomass (Fig. 15b). The maximum diatom

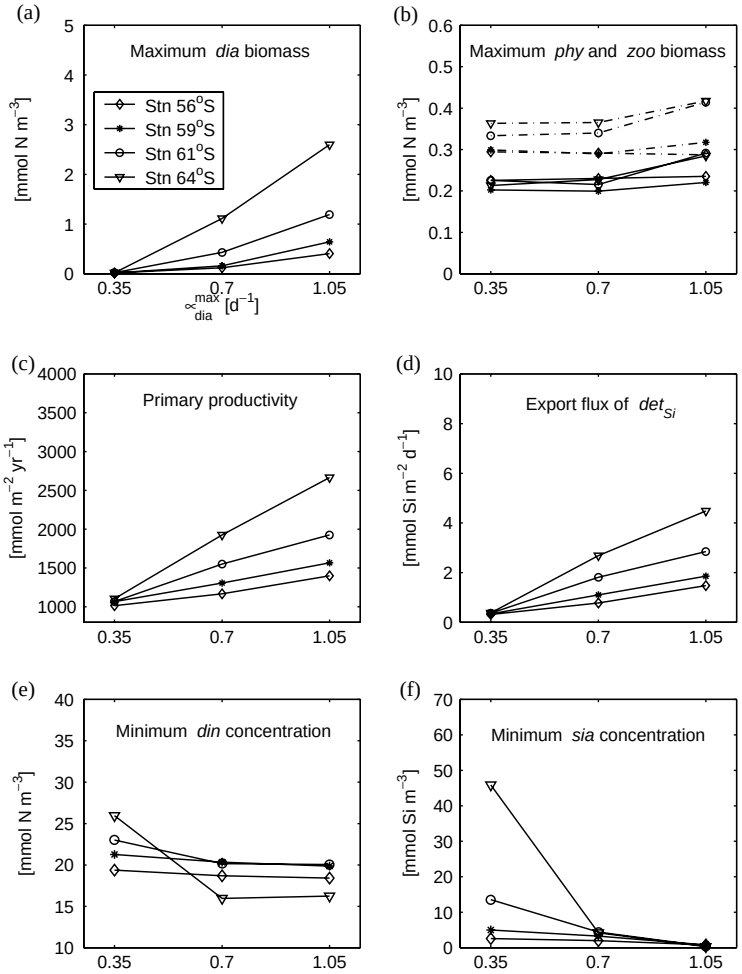

Fig. 15. Sensitivity of selected model diagnostics to variations of the maximum growth rate of diatoms. The solid lines in (b) represent small phytoplankton and the dash–dotted lines represent zooplankton.

biomass for $\mu_{dia}^{max} - 50\%$ is very low ($\sim$0.1 mmol N m^{-3}), and the nutrient drawdown is strongly reduced in this case, in particular at the two southernmost stations (Fig. 15e and f). The same model response is found for perturbations of the light parameter $\bar{\alpha}$ which also enters the parameterization of the diatom growth rate.

Perturbation of the maximum growth rate of small phytoplankton μ_{phy}^{max} also has a strong effect on the simulated primary production. The integrated primary productivity increases almost linearly by $\sim$700 mmol N m^{-2} yr^{-1} for an increase of μ_{phy}^{max} by 50%. The export flux, the maximum diatom biomass and the drawdown of silicic acid are not affected by variations of μ_{phy}^{max}. Interestingly the small phytoplankton biomass changes only slightly while the response in zooplankton is stronger (Fig. 16a). This illustrates the efficient "top-down" control of small phytoplankton productivity by grazing, which is provided by the strong coupling between small phytoplankton and zooplankton grazers. The increased phytoplankton production is cropped efficiently by quickly responding zooplankton, which accumulate while the small phytoplankton biomass remains at the same level.

Perturbation of the maximum grazing rate μ_{zoo}^{max} showed a qualitatively different, asymmetric

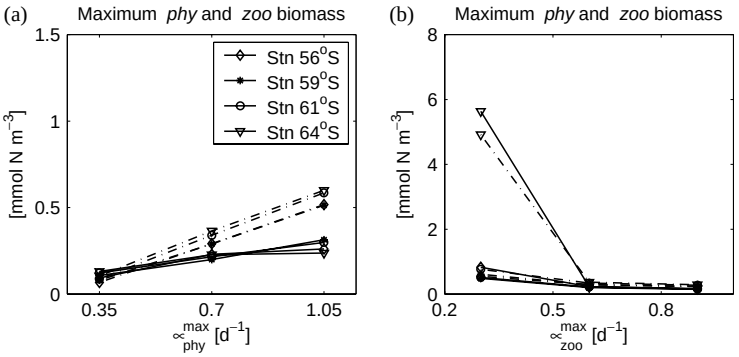

Fig. 16. Response of the maximum biomass of small phytoplankton (solid lines) and zooplankton (dash–dotted lines) to variations of the maximum growth rate of small phytoplankton in (a) and the maximum growth rate of zooplankton in (b).

response of the model. While increasing μ^{max}_{zoo} had no effect on the results, a decrease by 50% had a very pronounced effect on small phytoplankton and zooplankton biomass (Fig. 16b). The biomass of the small phytoplankton and zooplankton increases for the smaller grazing rate in particular at the two southern stations (Fig. 16b) and the drawdown of *din* increases as well. This case represents an "out of balance" coupling between the small phytoplankton and their grazers. An accumulation of small phytoplankton standing stocks is possible and occurs because the grazers do not respond quickly enough to control phytoplankton biomass.

Variations in the sinking velocity of diatoms and detritus primarily affect the export flux, which increases for higher sinking rates, and the maximum diatom biomass, which decreases. The model results show no sensitivity to the half-saturation concentration for nitrogen uptake k_N, as expected for the high dissolved inorganic nitrogen concentrations, or the loss rates of small phytoplankton and zooplankton L_{phy} and L_{zoo}. Variations of the loss rate of the diatoms L_{dia} lead to small responses in the maximum diatom biomass and the drawdown of inorganic nutrients. We did not observe a strong response to perturbations of the half-saturation concentration for silicic acid uptake k_{Si}. The minimum values of silicic acid increased at the southernmost station by about 4 mmol Si m^{-3} for each 50% reduction of k_{Si}, but the effect at the other stations is less pronounced. Variations in the remineralization rates r_N and r_{Si} only affect the export flux that increases for smaller remineralization rates.

In summary, the model is robust and no unexpected response to parameter perturbations occurred. The model results are most sensitive to variations of the maximum growth parameters and light parameters for which observation-based estimates exist. Less quantitative information is available on the maximum grazing rate, but we have chosen the parameter according to the qualitative picture of a strong coupling between phytoplankton and grazers. The results are not sensitive to the actual choice of the grazing parameter as long as it represents the region of strong grazer control in parameter space. If the grazing rate lies outside of this region, meaning the balance between primary producers and grazers is disturbed and "top-down" control is not important, small phytoplankton and zooplankton biomass increase considerably. Fortunately the model results are not sensitive to the loss parameters for which we have practically no quantitative information.

6. Summary and conclusions

We suggest a simple biochemical model for the pelagic system of the Southern Ocean that includes the cycling of silica and nitrogen, diatoms as a single functional group, and a tightly coupled balance between small phytoplankton and zooplankton. The model is applied to four stations in

different biogeochemical regions of the southwest Pacific sector, namely the Polar Frontal Zone north of the Polar Front (PF), the vicinity of the PF, and the Seasonal Ice Zone south of the PF. The employed set of biological parameters, based on observational and experimental estimates from the Southern Ocean, turned out to be applicable for the different biogeochemical systems. This suggests that the formulation can be applied in a 3D circulation model that spans the subsystems. Comparison of the simulations with observations shows that the essential features of the different subsystems are captured by the model, including the seasonal cycles of chlorophyll, dissolved inorganic nitrogen, silicic acid, biogenic silica, and primary production. Also, the increasing importance of diatoms toward the south and the patterns of vertical particle flux are simulated in agreement with observations.

In the model simulation the specific growth rate of the small phytoplankton increases in spring with the establishment of stratification and increasing solar radiation, but the standing stocks are controlled by efficient grazing. Zooplankton quickly respond to increased production and keep small phytoplankton biomass at stable, relatively low levels at all four stations. In contrast to the "top-down" control of small phytoplankton, the diatoms are regulated "bottom-up" by the available light and silicic acid concentrations and bloom in early summer when the light/mixing regime becomes favorable. The light conditions improve toward the south because the mixing depths are becoming shallower, and primary productivity and diatom biomass increase correspondingly. The increase in silicic acid concentrations toward the south is another important factor in determining diatom biomass and the amount of exported biogenic silica. It appears that the light/mixing conditions set the pace of the nutrient uptake while the available silicic acid (mainly determined by the initial concentrations before the start of the growing season) sets an upper limit on seasonal diatom production and export. The influence of variations in silicic acid concentrations and light on the diatom growth rate is illustrated in Fig. 17. The major seasonal fluctuation of the growth rate is due to variations in the photosynthetically available radiation at all four stations. The relative importance of silicic acid as a control of diatom productivity decreases along the latitudinal gradient toward the south. While the availability of silicic acid regulates diatom productivity at the northernmost station, it only temporarily reaches low enough values to limit the actual growth rates at the three southern stations.

The controls of the model-predicted primary productivity are different for the two phytoplankton groups and at the different stations. We identified three main controls: grazing, light availability, and silicic acid concentrations. The spatial differences in simulated patterns are mainly explained by variations in the light/mixing regime and the availability of silicic acid, which becomes temporarily important in late summer. Intense microzooplankton grazing is equally important at all stations in controlling standing stocks of small phytoplankton. The spatial and temporal switches between the controls of diatom productivity are subtle and emphasize that there is not a single ultimate control.

We invoke iron control implicitly by assuming growth rates that are typical for the low iron levels in the Southern Ocean. This approach turned out to be suitable for modeling the observed contemporary patterns. An increased supply of iron due to upwelling associated with the meandering PF has been suggested to explain higher chlorophyll levels in the vicinity of the PF (de Baar et al., 1995). In contrast to this hypothesis, our model captures the higher levels of chlorophyll in the vicinity of the PF without invoking an increase in specific growth due to higher iron supply. The temporarily favorable light conditions in the front result in higher chlorophyll levels in the model in agreement with the observed values. This is consistent with the findings of Arrigo et al. (1998) and Sambrotto and Mace (2000) who found that light availability is the main environmental factor determining productivity. If our model had failed to reproduce the seasonal pattern at the PF stations, this could have been interpreted as a corroboration of de Baar et al.'s hypothesis, but since our model results are in good agreement with the observations we cannot draw this conclusion.

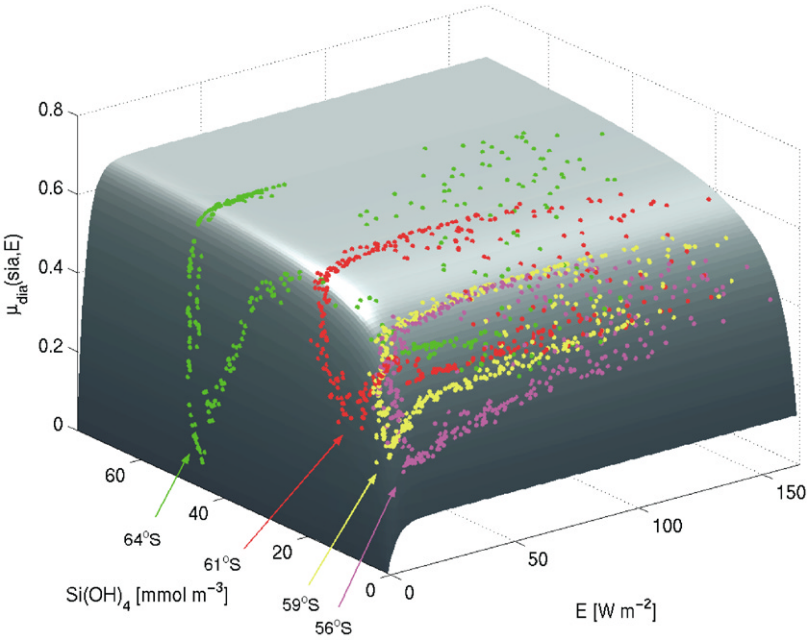

Fig. 17. The parameterization of the specific growth rate of the diatoms *dia* and its dependence upon silicic acid concentrations and photosynthetically available light is shown as gray surface. The colored symbols represent the range of specific growth rates actually reached during the model simulation at the different stations.

It is thought that higher airborne iron inputs during the Last Glacial Maximum resulted in a strong increase in primary productivity and export of carbon in the Southern Ocean (Moore et al., 2000; Martin, 1990). In a glacial model scenario the phytoplankton growth formulations, in particular the maximum growth rates, the light parameter, and the diatom stoichiometry, will have to be modified to take the effect of higher iron supply into account. In our sensitivity study, we explored the response of the model results to variations of the phytoplankton growth rates. An increase of the specific growth rates that would result from higher iron availability leads to increases in primary and export production and higher diatom biomass. Small phytoplankton biomass does not change for an increased growth rate since the small phytoplankton standing stock is controlled by zooplankton grazing but zooplankton biomass accumulates at higher levels. The model is most sensitive to variations in the phytoplankton growth rates, implying that changes in iron supply with subsequent changes in phytoplankton growth rates can have a substantial effect on primary productivity, biological structure, and carbon export.

Acknowledgements

We wish to thank Robert Anderson, Ekaterina Popova, Inga Hense and an anonymous reviewer for their thoughtful comments. This work has been supported by a grant from the National Aeronautics and Space Administration (NAG5-4947). US JGOFS contribution no. 716.

References

Abbott, M.R., Richman, J.G., Letelier, R.M., Bartlett, J.S., 2000. The spring bloom in the Antarctic Polar Frontal Zone as observed from a mesoscale array of bio-optical sensors. Deep-Sea Research II 47, 3285–3314.

Alldredge, A.L., Gottschalk, C.C., 1989. Direct observations of the mass flocculation in diatom blooms: characteristics,

settling velocities and formation of diatom aggregates. Deep-Sea Research II 36, 159–171.

Arrigo, K.R., Worthen, D., Schnell, A., Lizotte, M.P., 1998. Primary productivity in Southern Ocean waters. Journal of Geophysical Research 103 (8), 15587–15600.

Banse, K., 1996. Low seasonality of low concentrations of surface chlorophyll in the Subantarctic water ring: underwater irradiance, iron, or grazing? Progress in Oceanography 37, 241–291.

Barth, J.A., Cowles, T.J., Pierce, S.D., 2001. Mesoscale physical and bio-optical structure of the Antarctic Polar Front near 170°W during spring. Journal of Geophysical Research 106, 13.879–13.902.

Bathmann, U., Scharek, R., Klaas, C., Dubischar, C.D., Smetacek, V., 1997. Spring development of phytoplankton biomass and composition in major water masses of the Atlantic sector of the Southern Ocean. Deep-Sea Research II 44, 51–67.

Bathmann, U., Priddle, J., Trèguer, P., Lucas, M., Hall, J., Parslow, J., 2000. Plankton ecology and biogeochemistry in the Southern Ocean: a review of the Southern Ocean JGOFS. In: Hanson, R.B., Ducklow, H.W., Field, J.G. (Eds.), The Changing Ocean Carbon Cycle. Cambridge University Press, Cambridge, pp. 301–337.

Becquevort, S., 1997. Nanoprotozooplankton in the Atlantic sector of the Southern Ocean during early spring: Biomass and feeding activities. Deep-Sea Research II 44, 355–374.

Bienfang, P.K., 1980. Phytoplankton sinking rates in oligotrophic waters off Hawaii, USA. Marine Biology 61, 69–77.

Bienfang, P.K., 1981. Sinking rates of heterogeneous, temperate phytoplankton populations. Journal of Plankton Research 3, 235–253.

Bienfang, P.K., Harrison, P.J., Quarmby, L.M., 1982. Sinking rate response to depletion of nitrate, phosphate and silicate in four marine diatoms. Marine Biology 67, 295–302.

Boyd, P.W., et al., 2000. A mesoscale phytoplankton bloom in the polar Southern Ocean stimulated by iron fertilization. Nature 407, 695–702.

Brock, T.D., 1981. Calculating solar radiation for ecological studies. Ecological Modelling 14, 1–19.

Bruland, K.W., Silver, M.W., 1981. Sinking rates of fecal pellets from gelatinous zooplankton (salps, pteropods, doliolids). Marine Ecology Progress Series 63, 295–300.

Brzezinski, M.A., Nelson, D.M., Franck, V.M., Sigmon, D.E., 2001. Silicon dynamics within an intense open-ocean diatom bloom in the Pacific sector of the Southern Ocean. Deep-Sea Research II 48, 3997–4018.

Chan, A.T., 1980. Comparative physiological study of marine diatoms and dinoflagelates in relation to irradiance and cell size: II relationship between photosynthesis, growth, and carbon/chlorophyll a ratio. Journal of Phycology 16, 428–432.

Cullen, J.J., 1990. On models of growth and photosynthesis in phytoplankton. Deep-Sea Research I 37, 667–683.

Cullen, J.J., 1991. Hypotheses to explain high-nutrient conditions in the open sea. Limnology and Oceanography 36, 1578–1599.

Cullen, J.J., 1995. Status of the iron hypothesis after the Open-Ocean Enrichment Experiment. Limnology and Oceanography 40, 1336–1343.

Dagg, M., Urban-Rich, J., Peterson, J., 2003. The potential contribution of fecal pellets from large copepods to the flux of biogenic silica and particulate organic carbon in the Antarctic Polar Front region near 170°W, this issue (PII: S0967-0645(02)00107-9).

Daly, K.L., Smith, W.O., Johnson, G.C., DiTullio, G.R., ones, D.R., Mordy, C.W., Feely, R.A., Hansell, D.A., Zhang, J., 2001. Hydrography, nutrients, and carbon pools in the Pacific sector of the Southern Ocean: implications for carbon flux. Journal of Geophysical Research 106, 7107–7124.

de Baar, H.J.W., Boyd, P.W., 2000. The role of iron in plankton ecology and carbon dioxide transfer of the global oceans. In: Hanson, R.B., Ducklow, H.W., Field, J.G. (Eds.), The Changing Ocean Carbon Cycle. Cambridge University Press, Cambridge, pp. 412–415.

de Baar, H.J.W., Jong, J.T.M., Bakker, D.C.E., Löscher, B.M., Veth, C., Bathmann, U., Smetacek, V., 1995. Importance of iron for plankton blooms and carbon dioxide drawdown in the Southern Ocean. Nature 373, 412–415.

DeMaster, D.J., Dunbar, R.B., Gordon, L.I., Leventer, A.R., Morrison, J.M., Nelson, D.M., Nittrouer, C.A., Smith, W.O., 1992. The cycling and accumulation of organic matter and biogenic silica in high-latitude environments: The Ross Sea. Oceanography 5, 146–153.

Dower, K.M., Lucas, M.I., 1993. Photosynthesis-irradiance relationships and production associated with a warm-core ring shed from the Agulhas Retroflection south of Africa. Marine Ecology Progress Series 95, 141–154.

Dubischar, C.D., Bathmann, U., 1997. Grazing impact of copepods and salps on phytoplankton in the Atlantic sector of the Southern Ocean. Deep-Sea Research II 44, 415–433.

Duffie, J.A., Beckman, W.A., 1980. Solar Engineering of Thermal Processes. Wiley-Interscience, New York.

Dugdale, R.C., Wilkerson, F.P., Minas, H.J., 1995. The role of the silica pump in driving new production. Deep-Sea Research I 42, 697–719.

El-Sayed, S.Z., Taguchi, S., 1981. Primary production and standing crop of phytoplankton along the ice-edge in the Weddell Sea. Deep-Sea Research I 28, 1017–1032.

Fennel, K., Abbott, M.R., Spitz, Y.H., Richman, J.G., Nelson, D.M., 2003. Impacts of iron control on phytoplankton production in the modern and glacial Southern Ocean. Deep-Sea Research II, this issue (PII: S0967-0645(02)005969).

Fiala, M., Kopczynska, E.E., Jeandel, C., Oriol, L., Vetion, G., 1998. Seasonal and interannual variability of size-fractionated phytoplankton biomass and community structure at station KERFIX, off Kerguelen Islands. Journal of Plankton Research 20, 1256–1341.

Figueiras, F.G., Perez, F.F., Pazos, Y., Rios, A.F., 1994. Light and productivity of Antarctic phytoplankton during austral summer in an ice edge region in the Weddell-Scotia Sea. Journal of Plankton Research 16, 233–253.

Franck, V.M., Brzezinski, M.A., Coale, K., Nelson, D.M., 2000. Iron and silicic acid concentrations regulate Si uptake north and south of the Polar Frontal Zone in the Pacific Sector of the Southern Ocean. Deep-Sea Research II 47, 3315–3338.

Froneman, P., Phakomov, E., Perissinotto, R., McQuaid, C., 2000. Zooplankton structure and grazing in the Atlantic sector of the Southern Ocean in late austral summer 1993 Part 2. Biochemical zonation. Deep-Sea Research I 47, 1687–1702.

Frost, B., 1991. The role of grazing control in nutrient-rich areas of the open ocean sea. Limnology and Oceanography 36, 1616–1630.

Grenfell, T.C., Maykut, G.A., 1977. The optical properties of ice and snow in the Arctic basin. Journal of Glaciology 18 (90), 445–463.

Guest, P.S., Glendening, J.W., Davidson, K.L., 1995. An observational and numerical study of wind stress variations within marginal ice zones. Journal of Geophysical Research 100, 10887–10904.

Hense, I., Bathmann, U.V., Timmermann, R., 2000. Plankton dynamics in frontal systems of the Southern Ocean. Journal of Marine Systems 27, 235–252.

Honjo, S., 1990. Particle fluxes and modern sedimentation in the polar oceans. In: Smith, W.O. (Ed.), Polar Oceanography. Academic Press, New York, pp. 322–353.

Honjo, S., Francois, R.F., Manganini, S., Dymond, J., Collier, R., 2000. Particle fluxes to the interior of the Southern Ocean in the Western Pacific sector along 170°W. Deep-Sea Research II 47, 3521–3548.

Howard-Williams, C., Davis-Colley, R., Vincent, W.F., 1995. Optical properties of the coastal and oceanic waters off South Island, New Zealand: Regional variation. New Zealand Journal of Marine and Freshwater Research 29 (4), 589–602.

Hutchins, D.A., Bruland, K.W., 1998. Iron-limited diatom growth and Si:N uptake ratios in a coastal upwelling regime. Nature 393, 561–564.

Jacques, G., 1983. Some ecophysiological aspects of the Antarctic phytoplankton. Polar Biology 2, 27–33.

Jacques, G., Minas, M., 1981. Production primaire dans le secteur indien de l'Océan Antarctique an fin d'été. Oceanologica Acta 4, 33–41.

Jerlov, N.G., 1976. Marine Optics. Elsevier, Amsterdam, Netherlands.

Jochem, F.J., Mathot, S., Queguiner, B., 1995. Size-fractionated primary production in the open Southern Ocean in austral spring. Polar Biology 15, 381–392.

Kraus, E.B., 1972. Atmosphere-Ocean Interaction. Clarendon Press, Oxford, England.

Lancelot, C., Hannon, E., Becquevort, S., Veth, C., de Baar, H.J.W., 2000. Modeling phytoplankton blooms and carbon export production in the Southern Ocean: dominant controls by light and iron in the Atlantic sector in Austral spring in 1992. Deep-Sea Research I 47, 1621–1662.

Landry, M.R., Selph, K.E., Brown, S.L., Abbott, M.R., Measures, C.I., Vink, S., Allen, C.B., Calbert, A., Christensen, S., Nolla, H., 2002. Seasonal dynamics of phytoplankton in the Atlantic Polar Front region at 170°W. Deep-Sea Research II 48, 1843–1865.

Laubscher, R.K., Persimotto, R., McQuaid, C.D., 1993. Phytoplankton production and biomass at frontal zones of the Atlantic sector of the Southern Ocean. Polar Biology 13, 471–481.

Martin, J., 1990. Glacial-interglacial CO_2 change: the iron hypothesis. Paleoceanography 5, 1–13.

Martin, J., Fitzwater, S.E., 1988. Iron deficiency limits phytoplankton growth in the north-east Pacific Subarctic. Nature 331, 341–343.

Measures, C.I., Vink, S., 2001. Dissolved Fe in the upper waters of the Pacific sector of the Southern Ocean. Deep-Sea Research II 48, 3913–3941.

Mengelt, C., Abbott, M.R., Barth, J.A., Letelier, R.M., Measures, C.I., Vink, S., 2001. Phytoplankton pigment distribution in relation to the physics across the Antarctic Polar Front, 170°, during austral summer. Deep-Sea Research II 48, 4081–4100.

Minas, H.J., Minas, M., 1992. Net community production in High Nutrient Low Chlorophyll waters of the tropical and Antarctic Oceans: grazing vs. iron hypothesis. Oceanologica Acta 15, 145–162.

Mitchell, B.G., Brody, E.A., Holm-Hansen, O., McClain, C., Bishop, J., 1991. Light limitation of phytoplankton biomass and macronutrient utilization in the Southern Ocean. Limnology and Oceanography 36, 1662–1677.

Moore, J.K., Abbott, M.R., Richman, J.G., 1999a. Location and dynamics of the Antarctic Polar Front from satellite sea surface temperature data. Journal of Geophysical Research 104 (2), 3059–3073.

Moore, J.K., Abbott, M.R., Richman, J.G., Smith, W.O., Cowles, T.J., Coale, K.H., Gardner, W.D., Barber, R.T., 1999b. SeaWiFS satellite ocean color data from the Southern Ocean. Geophysical Research Letters 26 (10), 1465–1468.

Moore, J.K., Abbott, M.R., Richman, J.G., Nelson, D.M., 2000. The Southern Ocean at the last glacial maximum: a strong sink for atmospheric carbon dioxide. Global Biogeochemical Cycles 14 (1), 455–475.

Muggli, D., Lecourt, M., Harrison, P.J., 1996. Effects of iron and nitrogen source on the sinking rate, physiology and metal composition of an oceanic diatom from the subarctic Pacific. Marine Ecology Progress Series 132, 215–227.

Nelson, D.M., Dortch, Q., 1996. Silicic acid depletion and silicon limitation in the plume of the Mississippi river: evidence from kinetic studies in spring and summer. Marine Ecology Progress Series 136, 163–178.

Nelson, D.M., Gordon, L.I., 1982. Production and pelagic dissolution of biogenic silica in the Southern Ocean. Geochimica Cosmochimica Acta 46, 491–501.

Nelson, D.M., Trèguer, P., 1992. Role of silicon as a limiting nutrient to Antarctic diatoms: evidence from kinetic studies in the Ross Sea ice-edge zone. Marine Ecology Progress Series 80, 255–264.

Nelson, D.M., Brzezinski, M.A., Sigmon, D.E., Franck, V.M., 2001. A seasonal progression of Si limitation in the Pacific sector of the Southern Ocean. Deep-Sea Research II 48, 3973–3995.

Nelson, D.M., et al., 2002. Vertical budgets of organic carbon and biogenic silica in the Pacific sector of the Southern Ocean, 1996–1998. Deep-Sea Research II 49, 1645–1674.

Orsi, A.H., Witworth, T., Nowlin, W.D., 1995. On the meridional extent and fronts of the Antarctic Circumpolar Current. Deep-Sea Research I 42, 641–673.

Payne, R.E., 1972. Albedo at the sea surface. Journal of Atmospheric Science 29, 959–970.

Perissinotto, R., Gurney, L., Phakomov, E., 2000. Contribution of heterotrophic material to diet and energy budget of Antarctic krill, Euphausia superba. Marine Biology 136, 129–135.

Platt, T., Gallegos, C.L., Harrison, W.G., 1980. Photoinhibition of photosynthesis in natural assemblages of marine phytoplankton. Journal of Marine Research 38, 687–701.

Platt, T., Rao, D.V.S., Smith, J.C., Li, W.K., Irwin, B., Horne, E.P.W., Sameoto, D.D., 1983. Photosynthetically-competent phytoplankton from the aphotic zone of the deep ocean. Marine Ecology Progress Series 10, 105–110.

Pondaven, P., Fravalo, C., Ruiz-Pino, D., Trèguer, P., Queguiner, B., Jeandel, C., 1998. Modelling the silica pump in the Permanently Open Ocean Zone of the Southern Ocean. Journal of Marine Systems 17, 587–619.

Pondaven, P., Ruiz-Pino, D., Fravalo, C., Trèguer, P., Jeandel, C., 2000. Interannual variability of Si and N cycles at the time-series station KERFIX between 1990 and 1995—a modelling study. Deep-Sea Research I 47, 223–257.

Price, J.F., Weller, R.A., Pinkel, R., 1986. Diurnal cycling: observations and models of the upper ocean response to diurnal heating, cooling, and wind mixing. Journal of Geophysical Research 91, 8411–8427.

Razouls, S., Reau, G.D., Guillot, P., Maison, J., Jeandel, C., 1998. Seasonal abundance of copepods and grazing pressure in the Kerguelen Island area (Southern Ocean). Journal of Plankton Research 20, 1599–1614.

Sakshaug, E., Kiefer, D.A., Andresen, K., 1989. A steady state description of growth and light absorption in the marine planktonic diatom skeletonema costatum. Limnology and Oceanography 34, 198–205.

Sambrotto, R.N., Mace, B.J., 2000. Coupling of biological and physical regimes across the Antarctic Polar Front as reflected by nitrogen and recycling. Deep-Sea Research II 47, 3339–3367.

Scharek, R., van Leeuwe, M.A., de Baar, H.J.W., 1997. Responses of Southern Ocean phytoplankton to the addition of trace metals. Deep-Sea Research II 44, 209–227.

Smetacek, V., 1984. The supply of food to the benthos. In: Fasham, M.J. (Ed.), Flows of Energy and Materials in Marine Ecosystems: Theory and Practice. Plenum Press, New York, pp. 517–548.

Smetacek, V., 1985. Role of sinking in diatom life-history cycles: ecological, evolutionary and geological significance. Marine Biology 84, 239–251.

Smith, W.O., Nelson, D.M., Mathot, S., 1999. Phytoplankton growth rates in the Ross Sea, Antarctica, determined by independent methods: temporal variations. Journal of Plankton Research 21, 1519–1536.

Sommer, U., 1986. Nitrate- and silicate-competition among antarctic phytoplankton. Marine Biology 91, 345–351.

Steele, J., Henderson, E., 1992. The role of predation in plankton models. Journal of Plankton Research 14, 157–172.

Sullivan, C.W., 1986. Silicification by diatoms. In Silicon Biochemistry, Wiley, New York, pp. 59–89.

Takeda, S., 1998. Influence of iron availability on nutrient consumption ratio of diatoms in oceanic waters. Nature 393, 774–777.

Trèguer, P., Jacques, G., 1992. Dynamics of nutrients and phytoplankton, and fluxes of carbon, nitrogen and silicon in the Antarctic ocean. Polar Biology 12, 149–162.

Trèguer, P., Kamatani, A., Gueneley, S., Quèguiner, B., 1989. Kinetics of dissolution of Antarctic diatom frustules and the biogeochemical cycle of silicon in the Southern Ocean. Polar Biology 9, 397–403.

Urban-Rich, J., Dagg, M., Peterson, J., 2001. Copepod grazing on phytoplankton in the Pacific sector of the Antarctic Polar Front. Deep-Sea Research II 48, 4223–4246.

Verity, P.G., Smetacek, V., 1996. Organism life cycles, predation, and the structure of marine pelagic ecosystems. Marine Ecology Progress Series 130, 277–293.

Wilson, D.L., Smith, W.O., Nelson, D.M., 1986. Phytoplankton bloom dynamics of the western Ross Sea ice edge-I. Primary productivity and species-specific production. Deep-Sea Research I 33, 1375–1387.